Cell Genomics, Volume *4*

Supplemental information

Karyotypic stasis and swarming influenced the evolution of viral tolerance in a species-rich bat radiation

Nicole M. Foley, Andrew J. Harris, Kevin R. Bredemeyer, Manuel Ruedi, Sebastien J. Puechmaille, Emma C. Teeling, Michael F. Criscitiello, and William J. Murphy

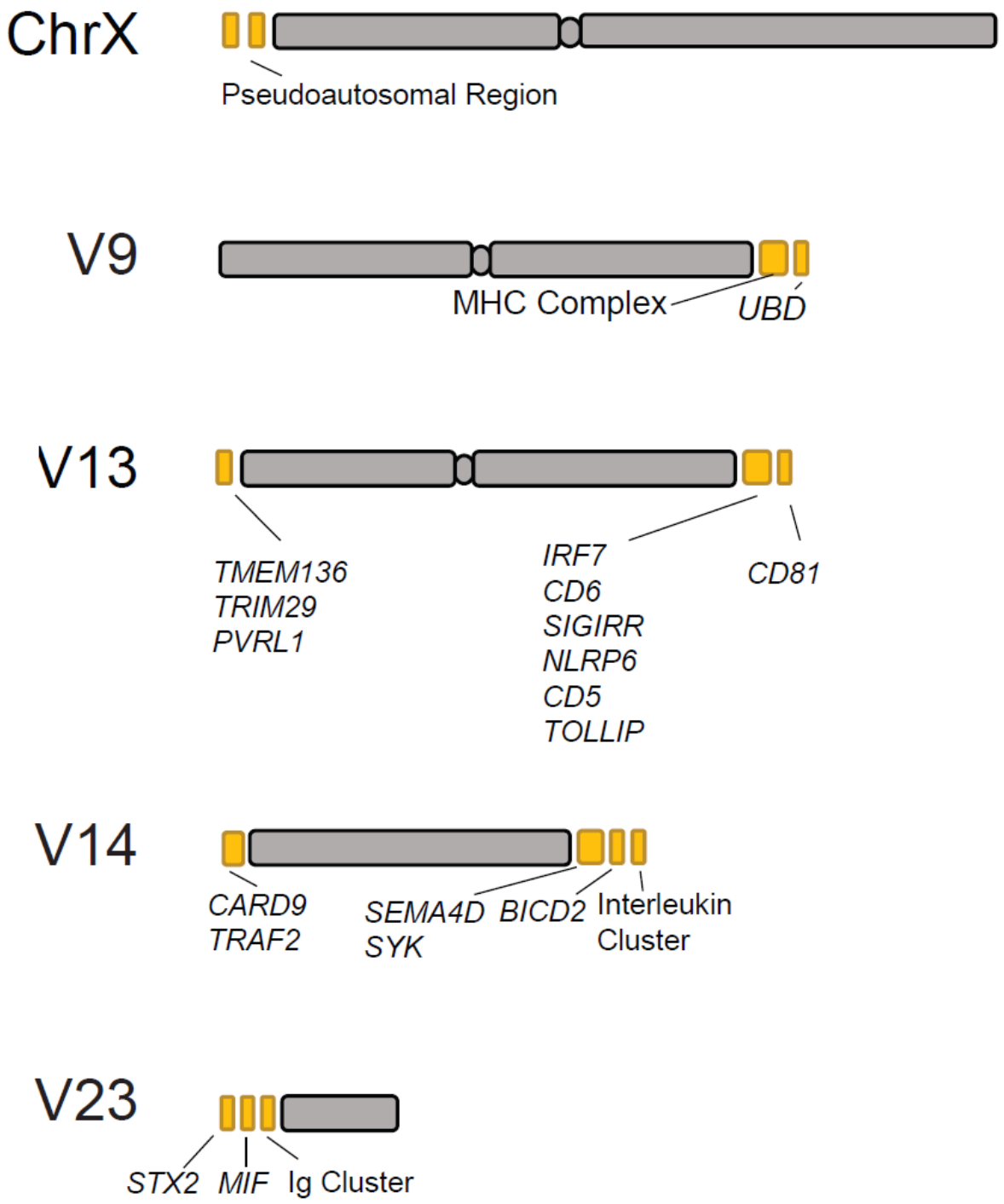

Figure S1: Previously unplaced assembly scaffolds contained many immune-related genes, related to the improved *Myotis myotis* genome assembly analyzed in Figure 2. Gray blocks depict the original chromosome-scale scaffolds from the original assembly (GCA_014108235.1). Yellow blocks represent unplaced scaffolds currently assigned to chromosomes. The yellow blocks are not drawn to scale.

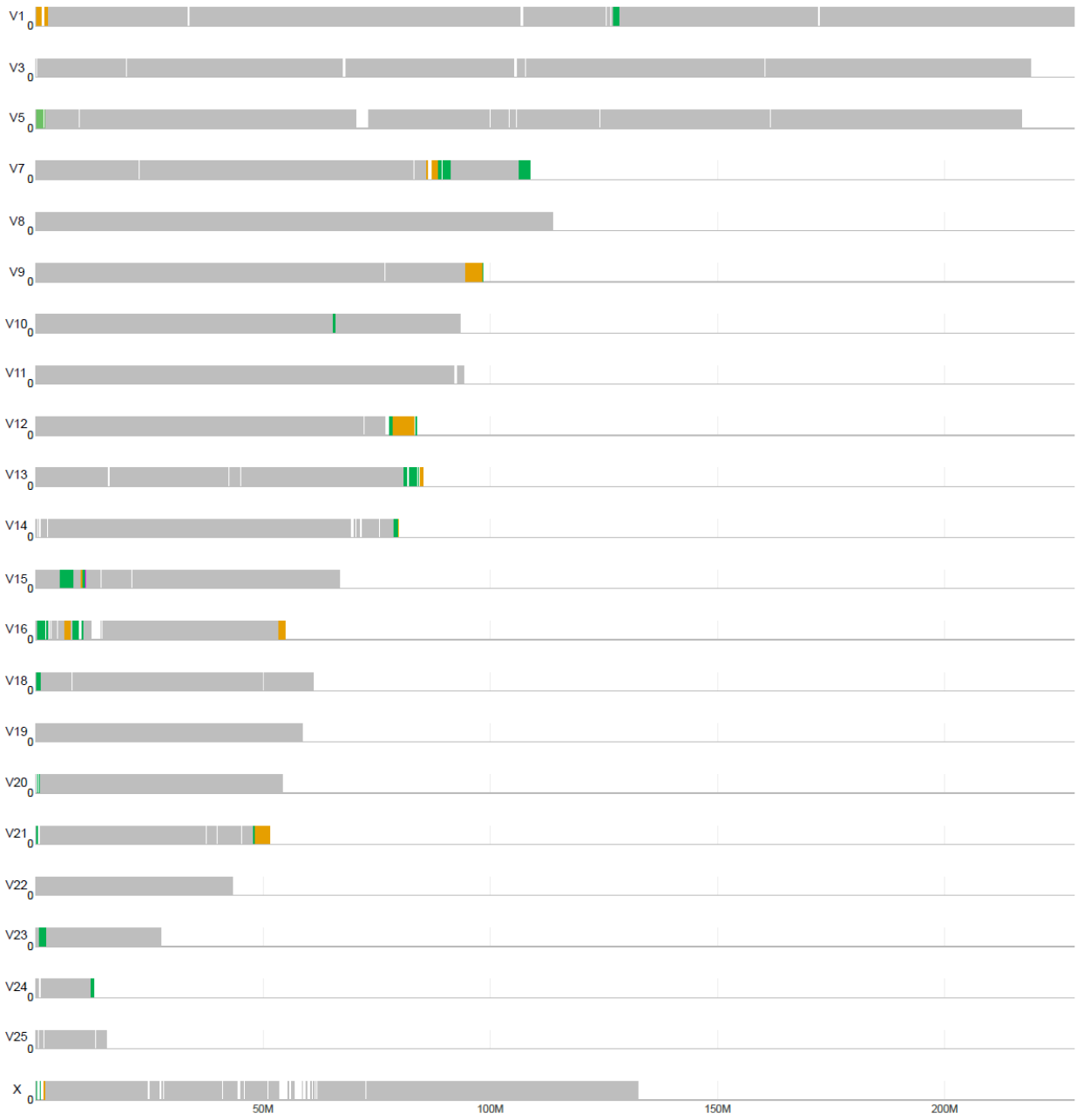

Figure S2: Most unplaced scaffolds were added to the terminal ends of chromosomes, related to the improved *Myotis myotis* genome analyzed in Figure 2. Portions of chromosomes colored gray represents the chromosome level scaffolds from the original assembly [S1]. Green and orange blocks, alternated to highlight where multiple scaffolds were added to the same region, illustrate where previously unplaced scaffolds were positioned in the new assembly based on Hi-C analysis and visualization in JBAT. All blocks and chromosomes are shown to scale. White spaces in blocks correspond to regions that were unassembled or removed due to missing data or poor alignment quality in the sliding window analysis.

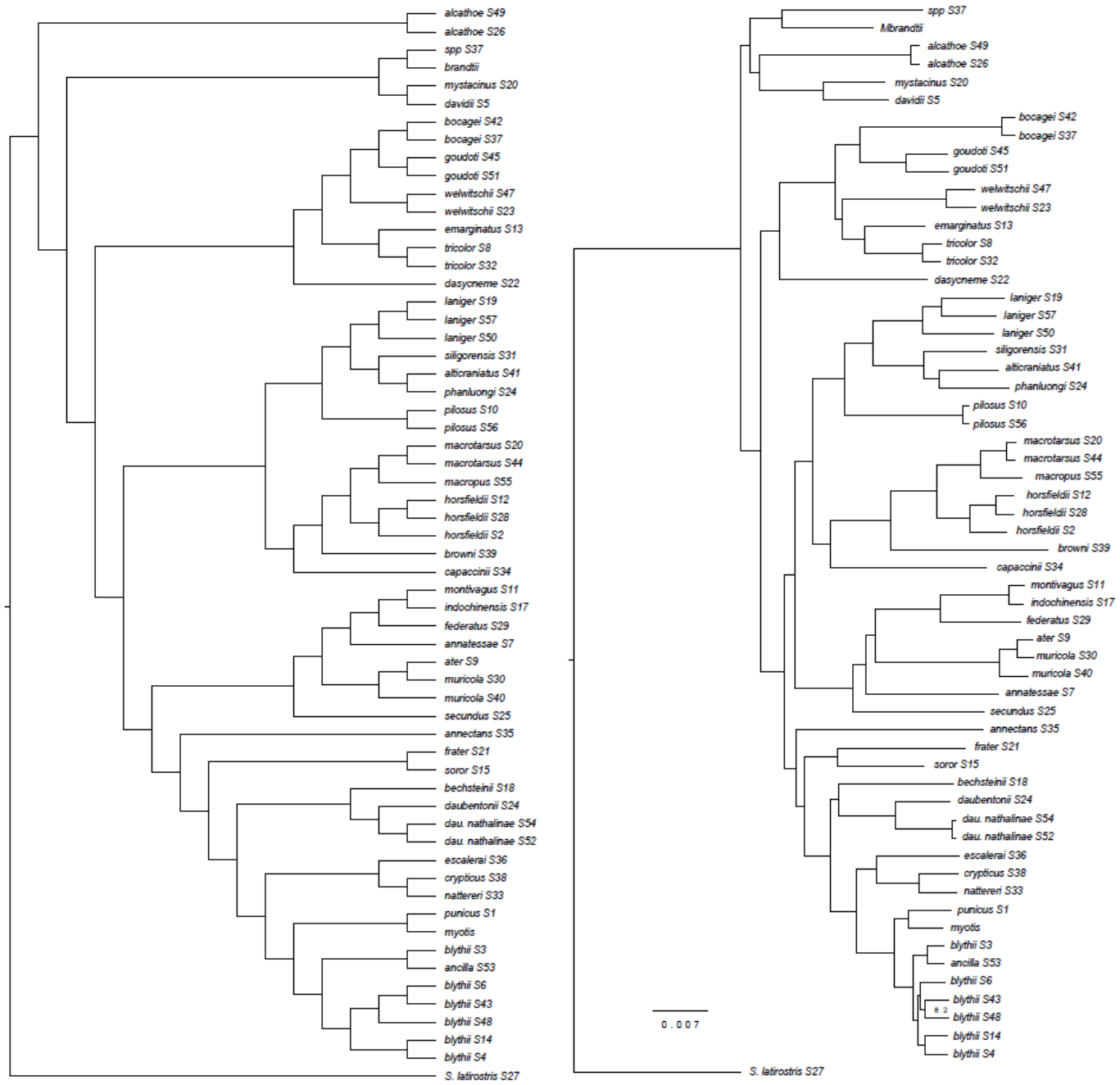

Figure S3: Whole genome nuclear topologies with all 60 individuals, related to Figure 1. The tree on the left is the 50% Majority Rule tree derived from the SVDquartets analysis. The rightmost tree is the IQtree2 Maximum Likelihood with branch lengths. All bootstrap supports are 100 unless otherwise indicated.

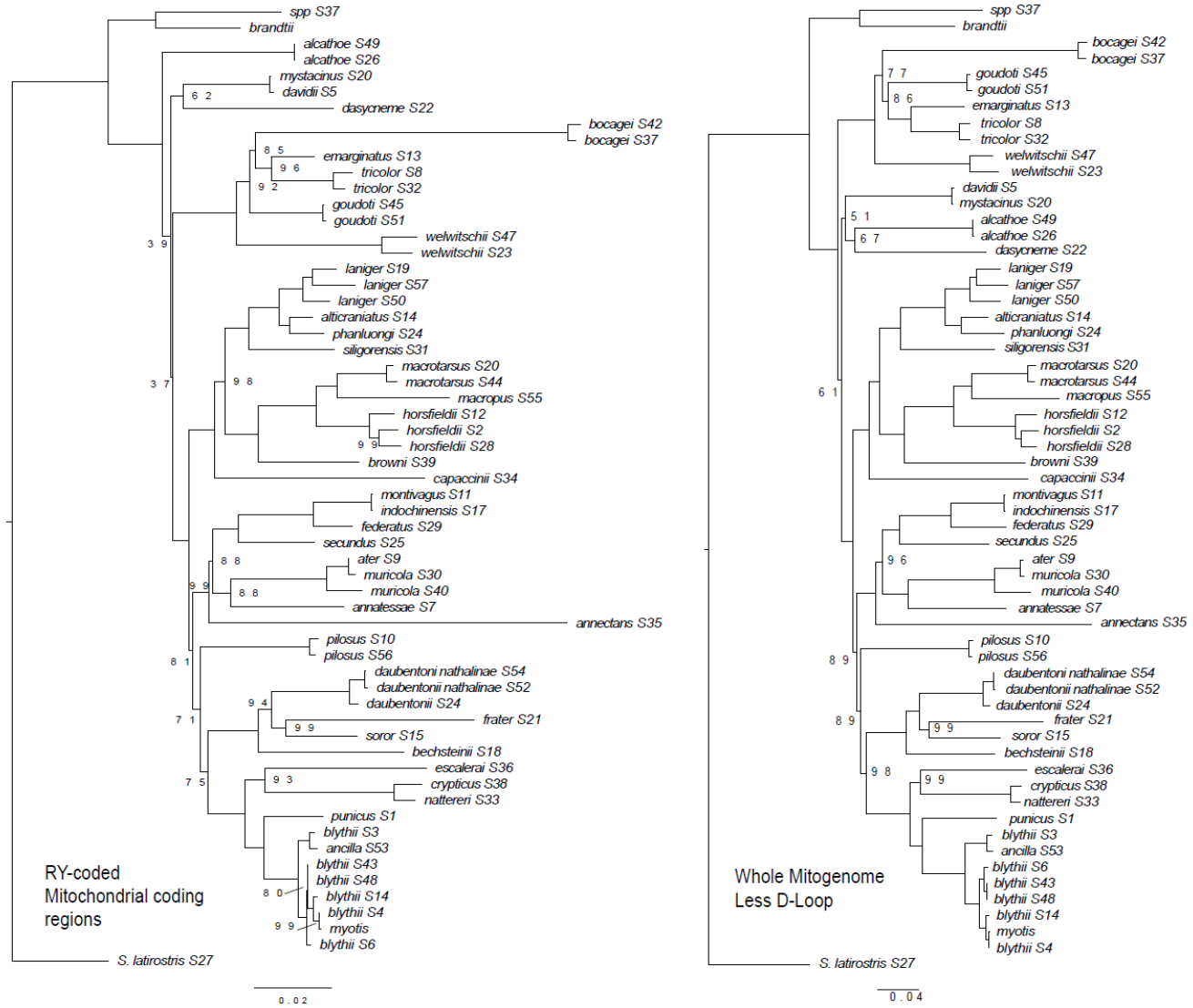

Figure S4: Mitogenome topologies with all 60 individuals, related to Figure 1. The tree on the left is RY-coded dataset. The tree on the right is the whole mitogenome with the D-Loop removed. All bootstrap supports are 100 unless otherwise indicated.

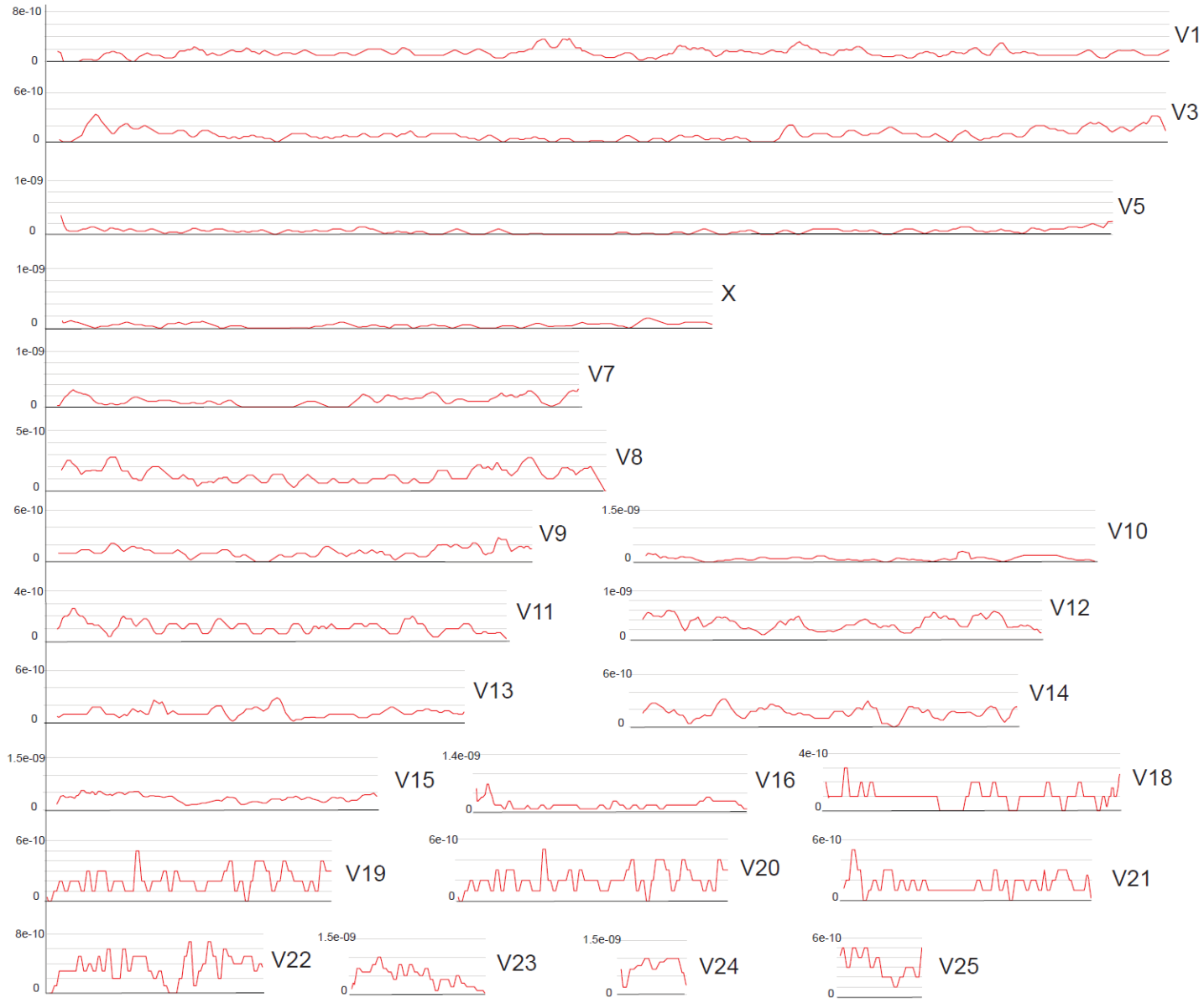

Figure S5.
***Myotis myotis* recombination map, related to Figure 2.** Genome-wide distribution of recombination rates inferred using ReLERNN. Rates are averaged every 2Mb in 50kb sliding windows. For illustrative purposes V1-V15 and chrX are displayed using a sliding average with a step of 50. Chromosomes V16-V25 are displayed using a sliding average with a step of 10.

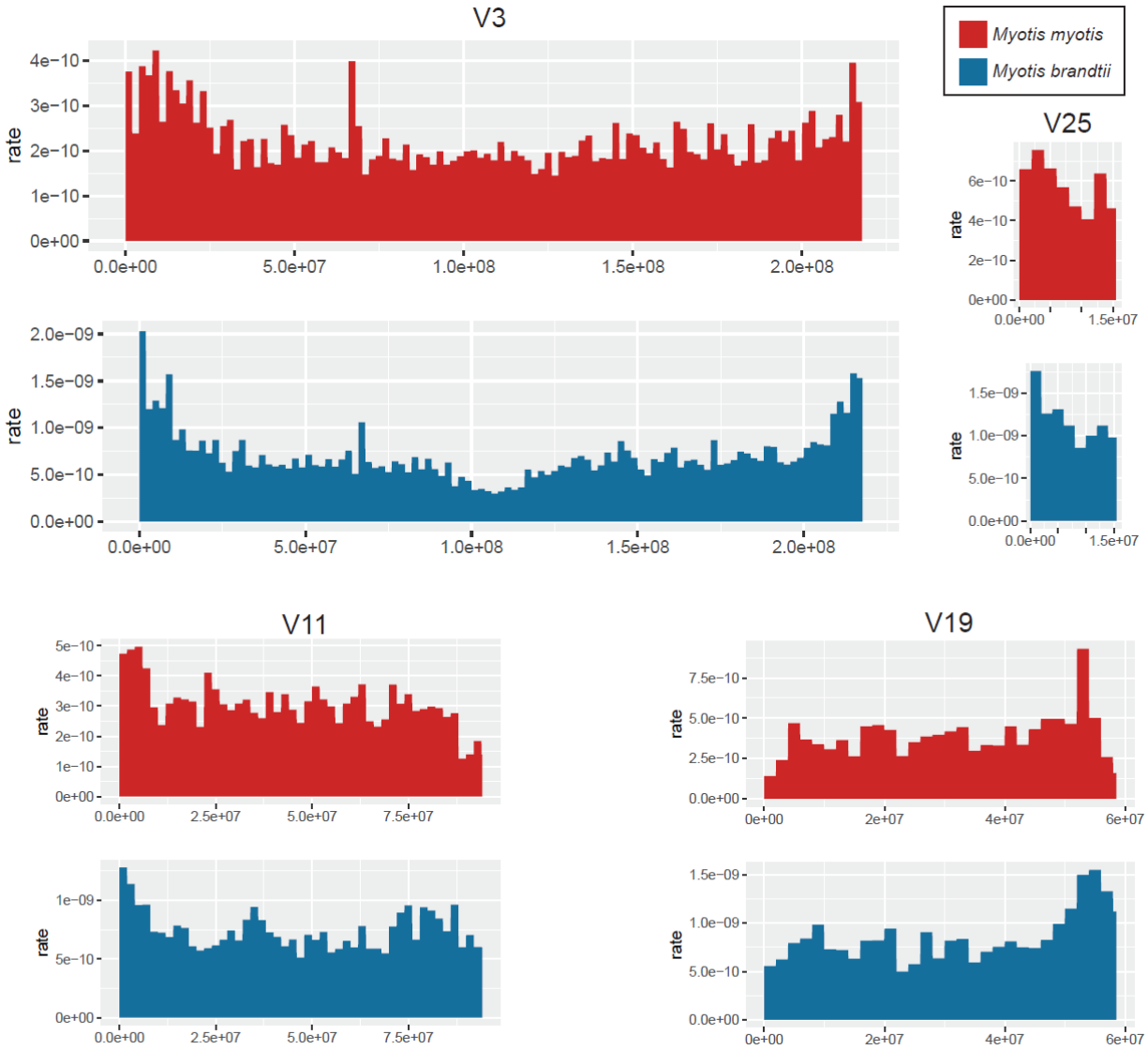

Figure S6: Comparison of select chromosomes from *M. myotis* and *M. brandtii* recombination maps, related to Figure 2.

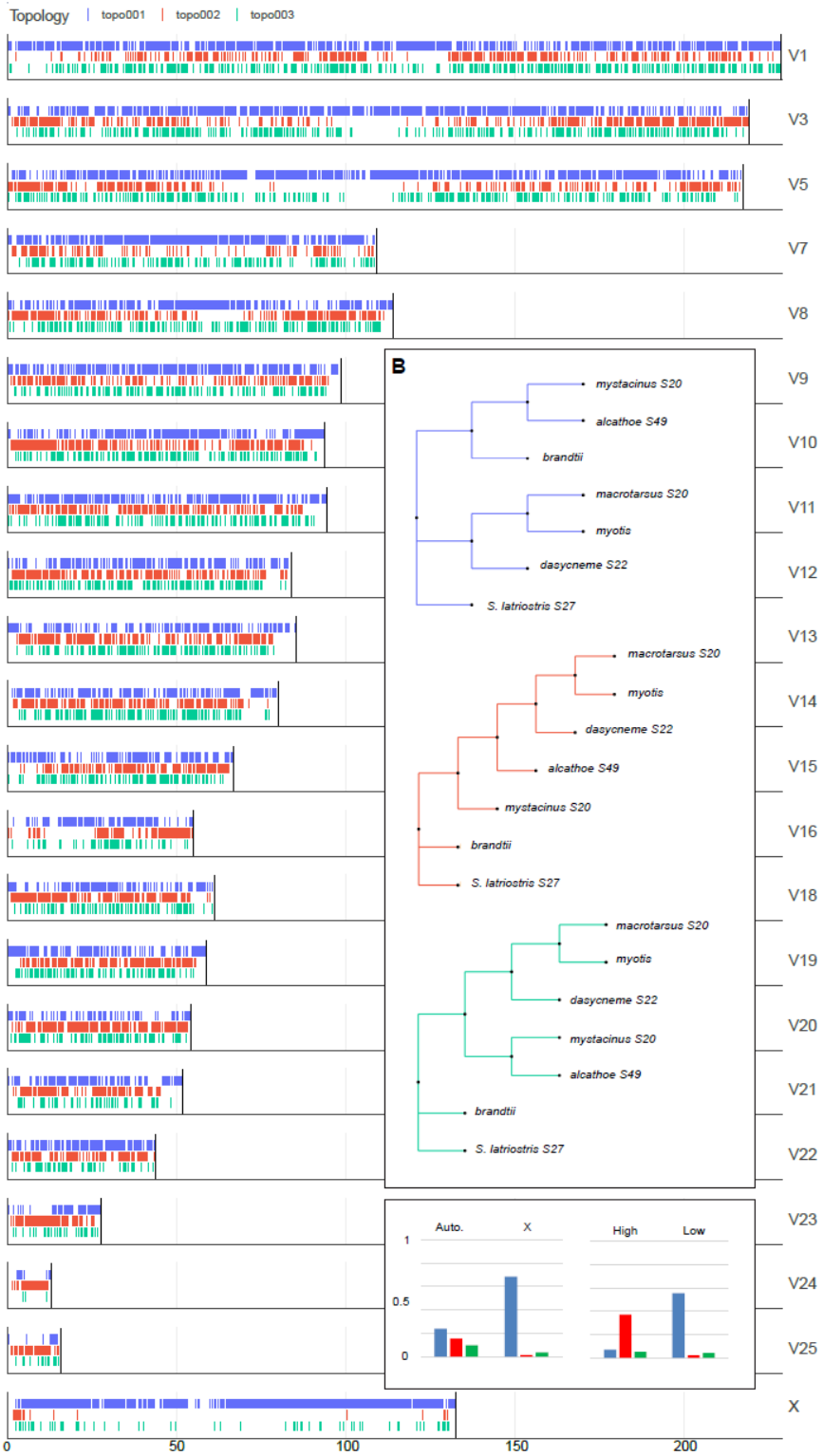

Figure S7: Genome-wide phylogenomic signal to determine the position of the whiskered bat clade, related to Figure 3. A) Genome-wide distribution of topologies shown in B). C) shows the frequency of each topology on the autosomes and X and in high and low recombining regions.

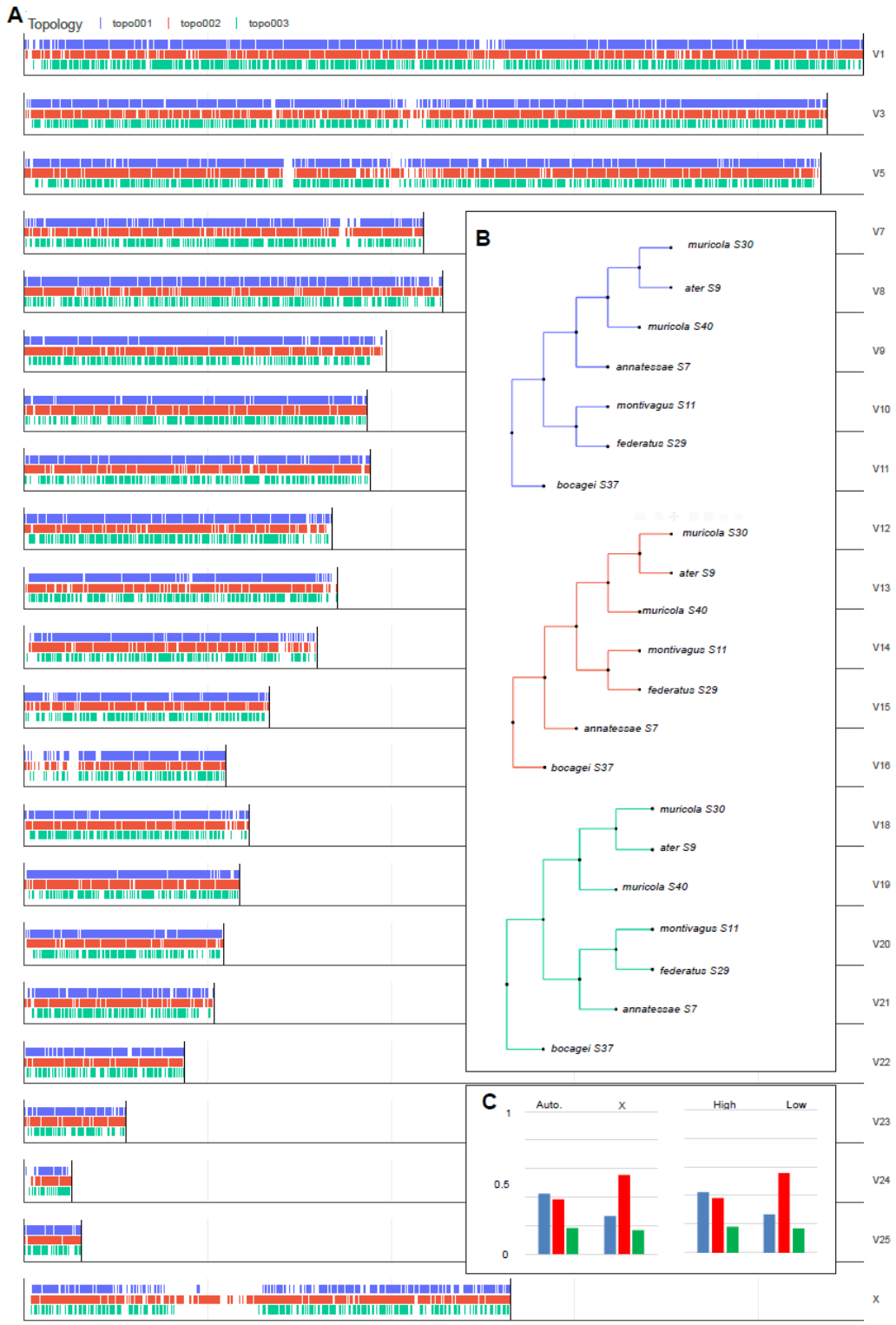

Figure S8: Genome-wide phylogenomic signal to determine the position of *M. annatessae*, related to Figure 3. A) Genome-wide distribution of topologies shown in B). C) shows the frequency of each topology on the autosomes and X and in high and low recombining regions.

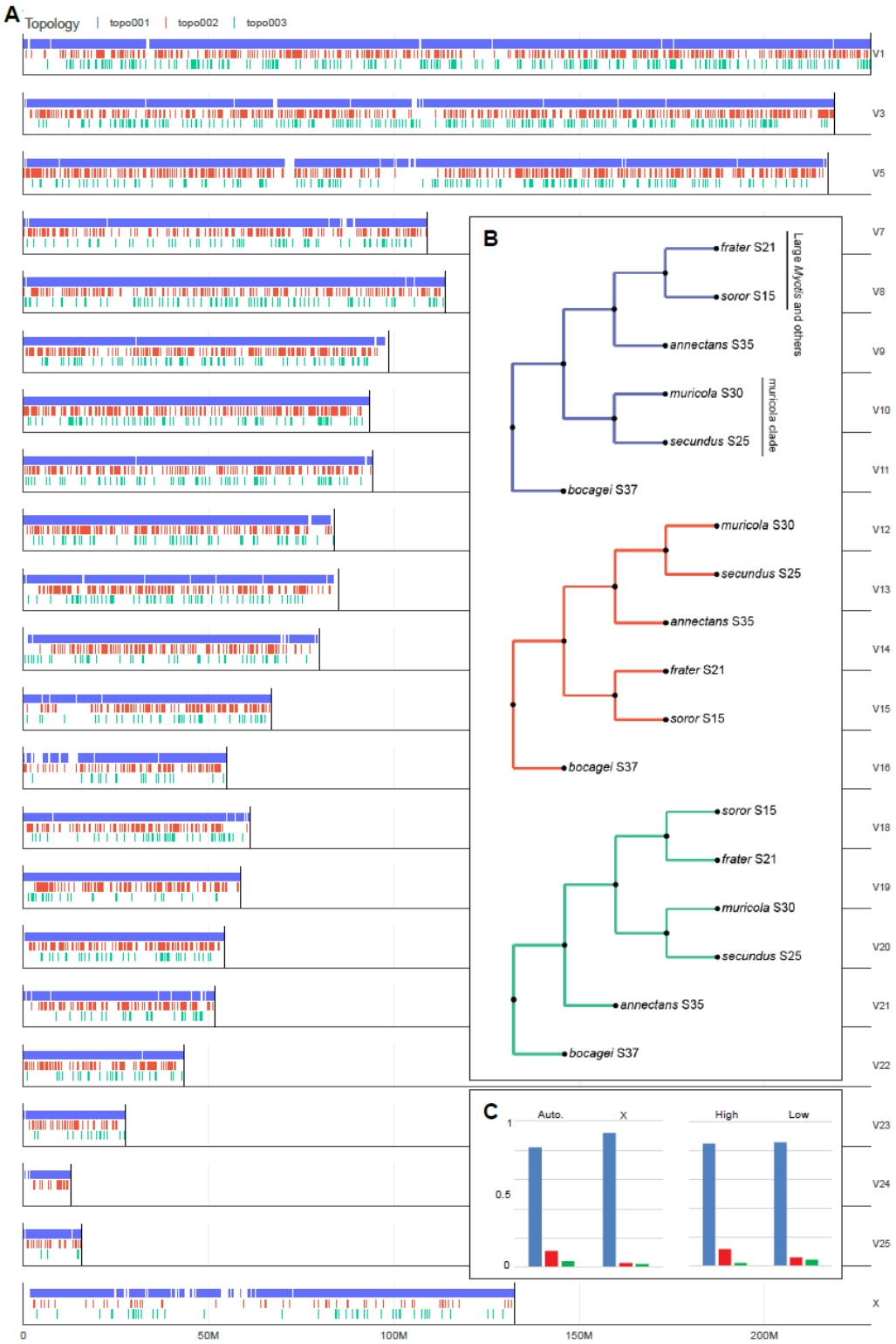

Figure S9: Genome-wide phylogenomic signal to determine the position of *M. annectans*, related to Figure 3. A) Genome-wide distribution of topologies shown in B). C) shows the frequency of each topology on the autosomes and X and in high and low recombining regions.

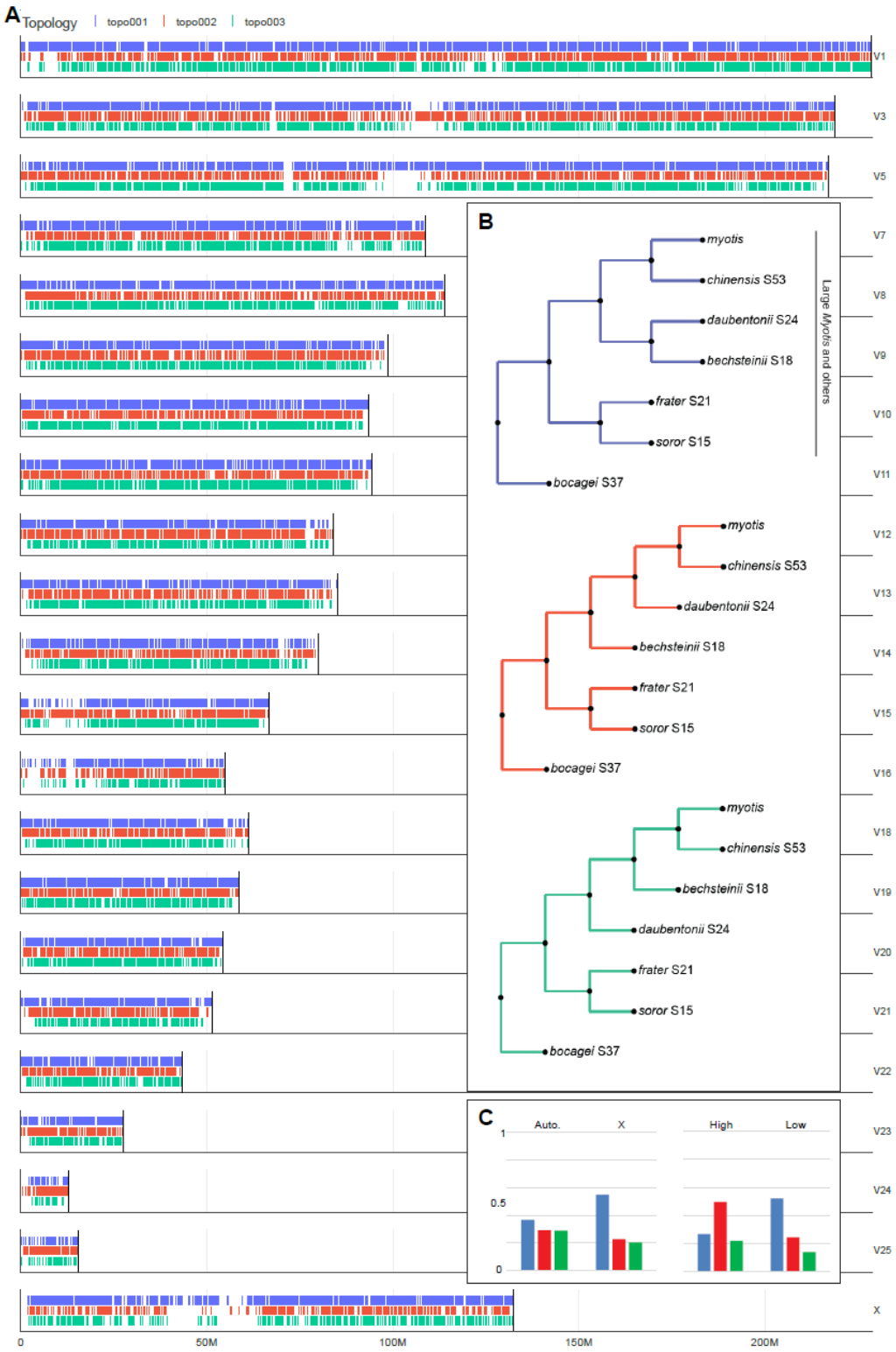

Figure S10: Genome-wide phylogenomic signal to determine the position of *M. bechsteinii*, related to Figure 3. A) Genome-wide distribution of topologies shown in B). C) shows the frequency of each topology on the autosomes and X and in high and low recombining regions.

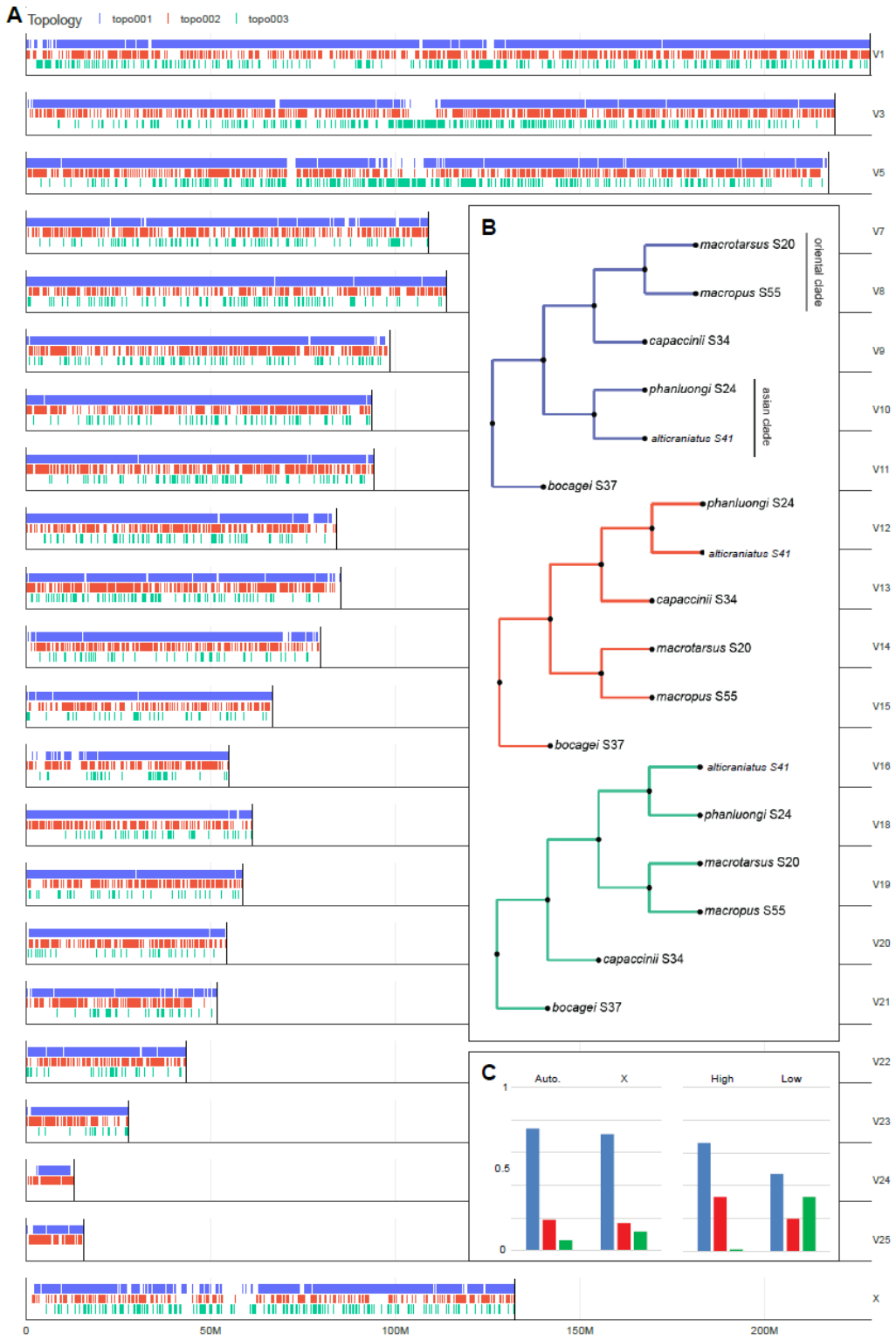

Figure S11: Genome-wide phylogenomic signal to determine the position of *M. capaccinii*, related to Figure 3. A) Genome-wide distribution of topologies shown in B). C) shows the frequency of each topology on the autosomes and X and in high and low recombining regions.

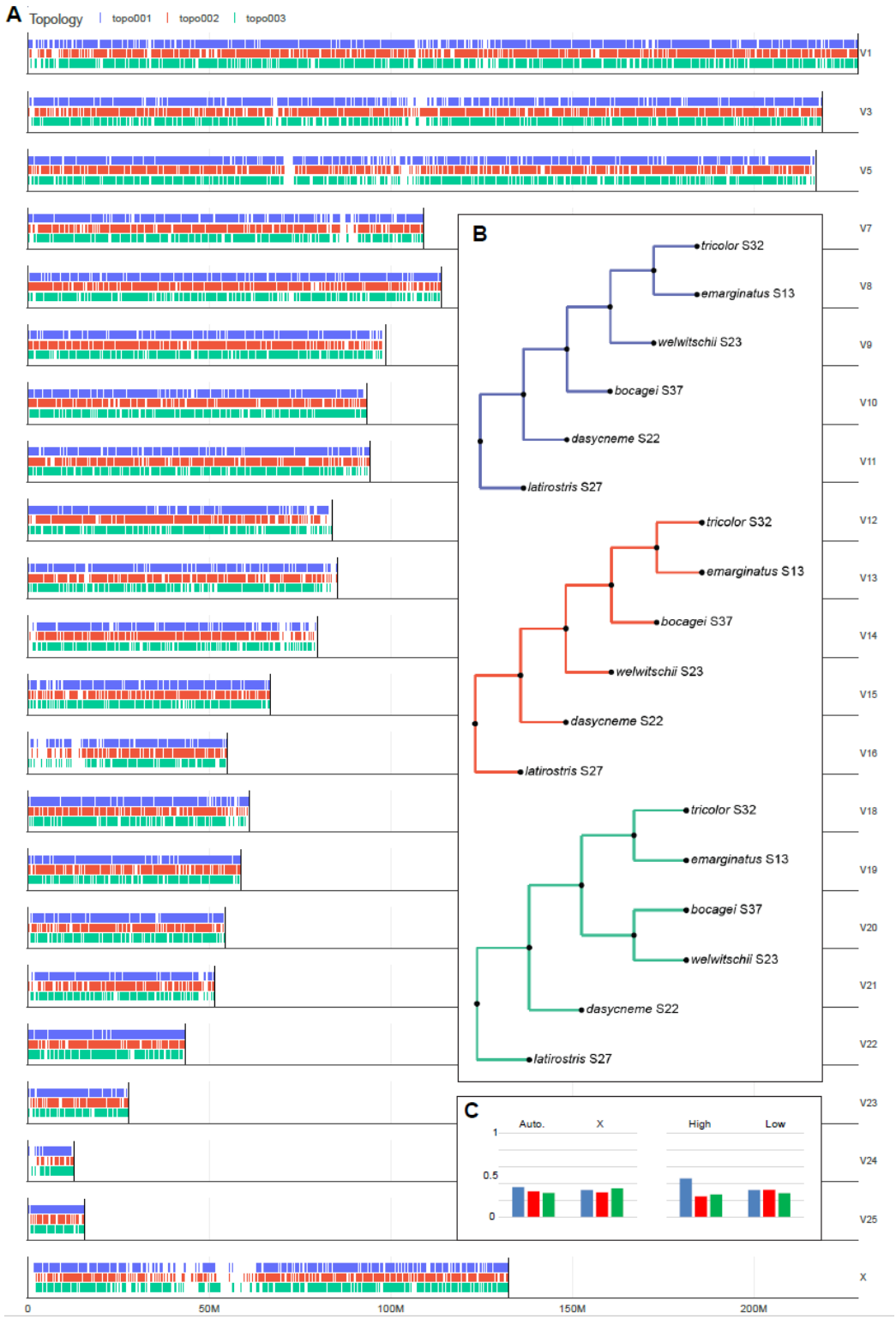

Figure S12: Genome-wide phylogenomic signal to determine the relationships among species in the Ethiopian clade, related to Figure 3. A) Genome-wide distribution of topologies shown in B). C) shows the frequency of each topology on the autosomes and X and in high and low recombining regions.

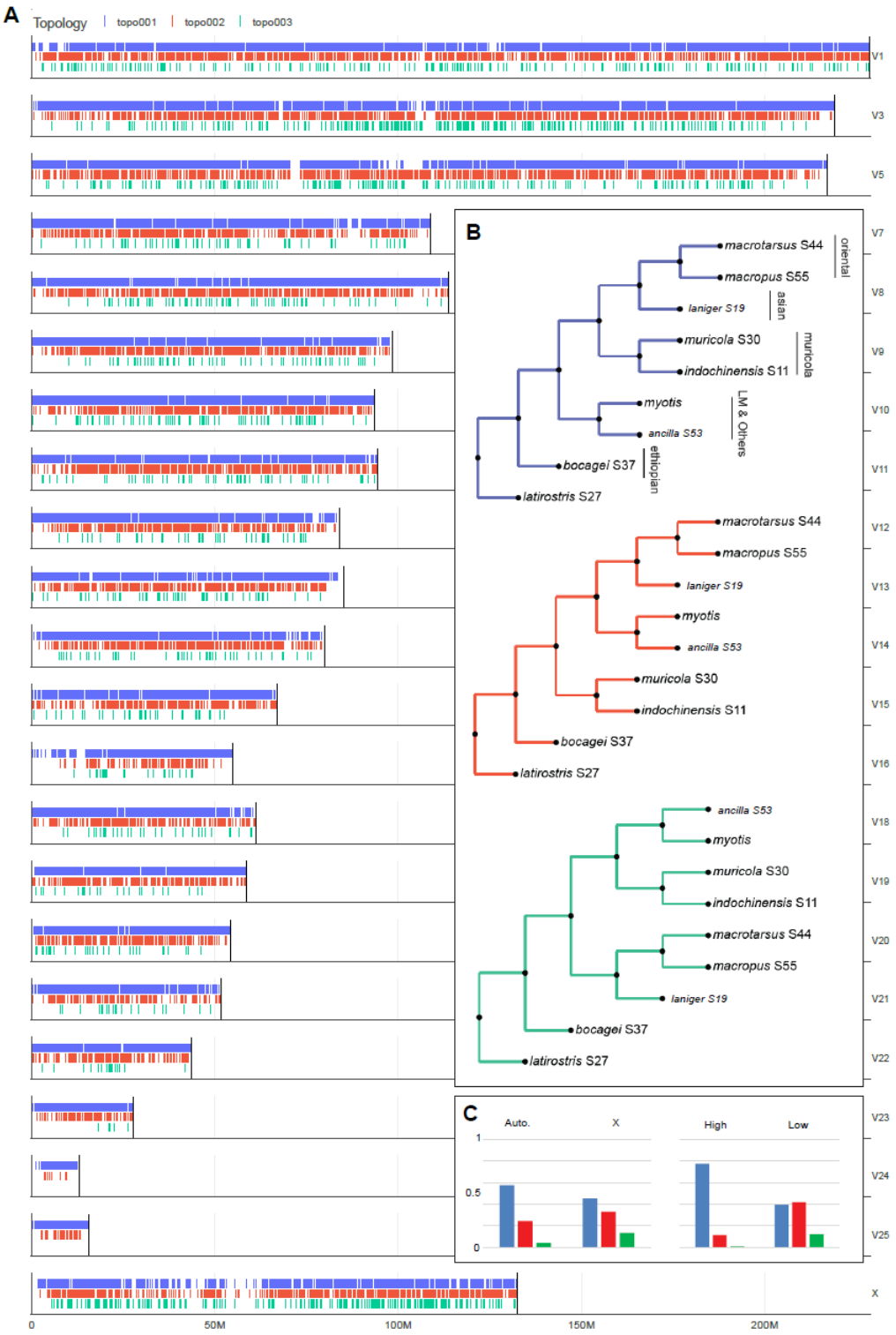

Figure S13: Genome-wide phylogenomic signal to determine the relationships among the major Old World Clades, related to Figure 3. A) Genome-wide distribution of topologies shown in B). C) shows the frequency of each topology on the autosomes and X and in high and low recombining regions.

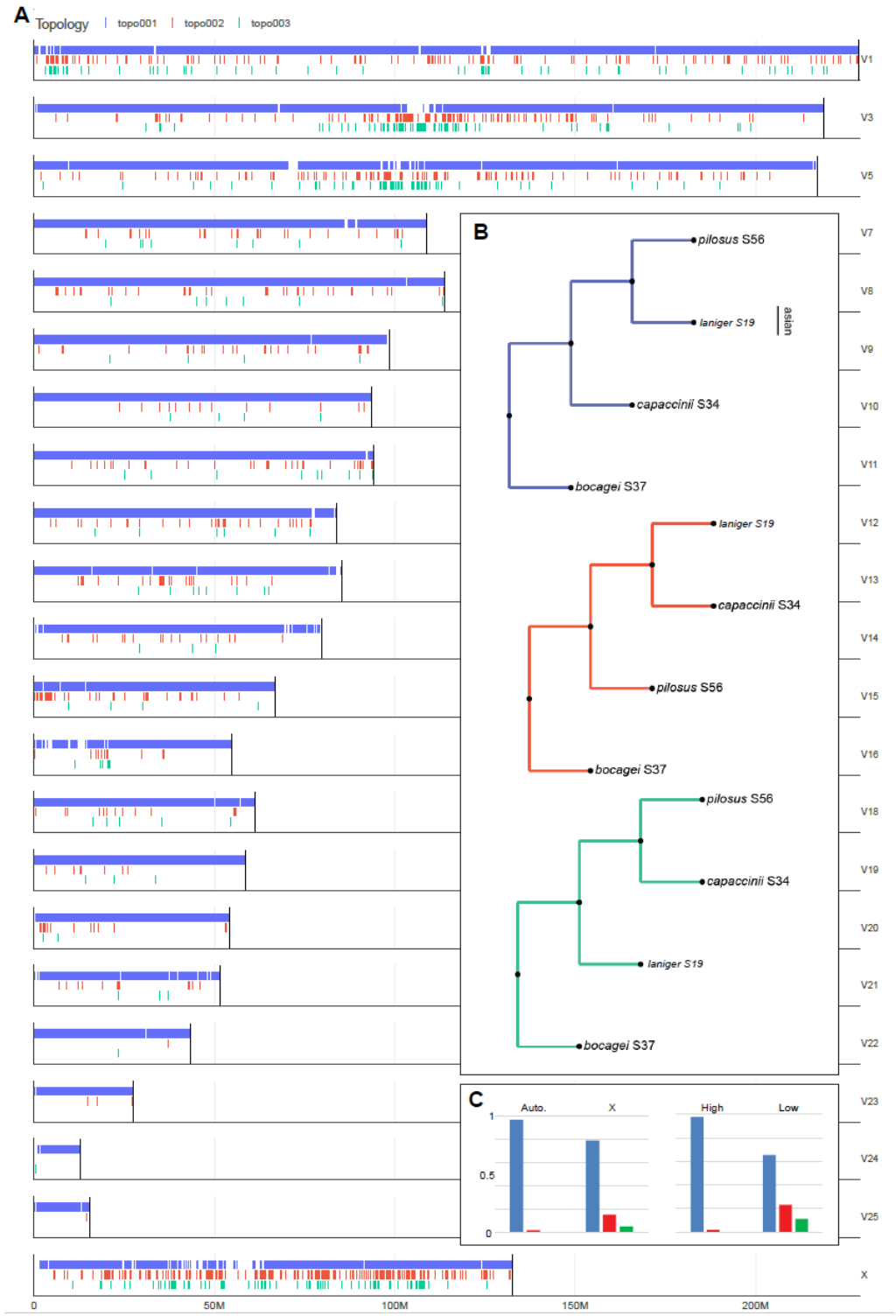

Figure S14: Genome-wide phylogenomic signal to determine the relationship between *M. pilosus*, *M. capaccinii* and *M. laniger*, related to Figure 3. A) Genome-wide distribution of topologies shown in B). C) shows the frequency of each topology on the autosomes and X and in high and low recombining regions.

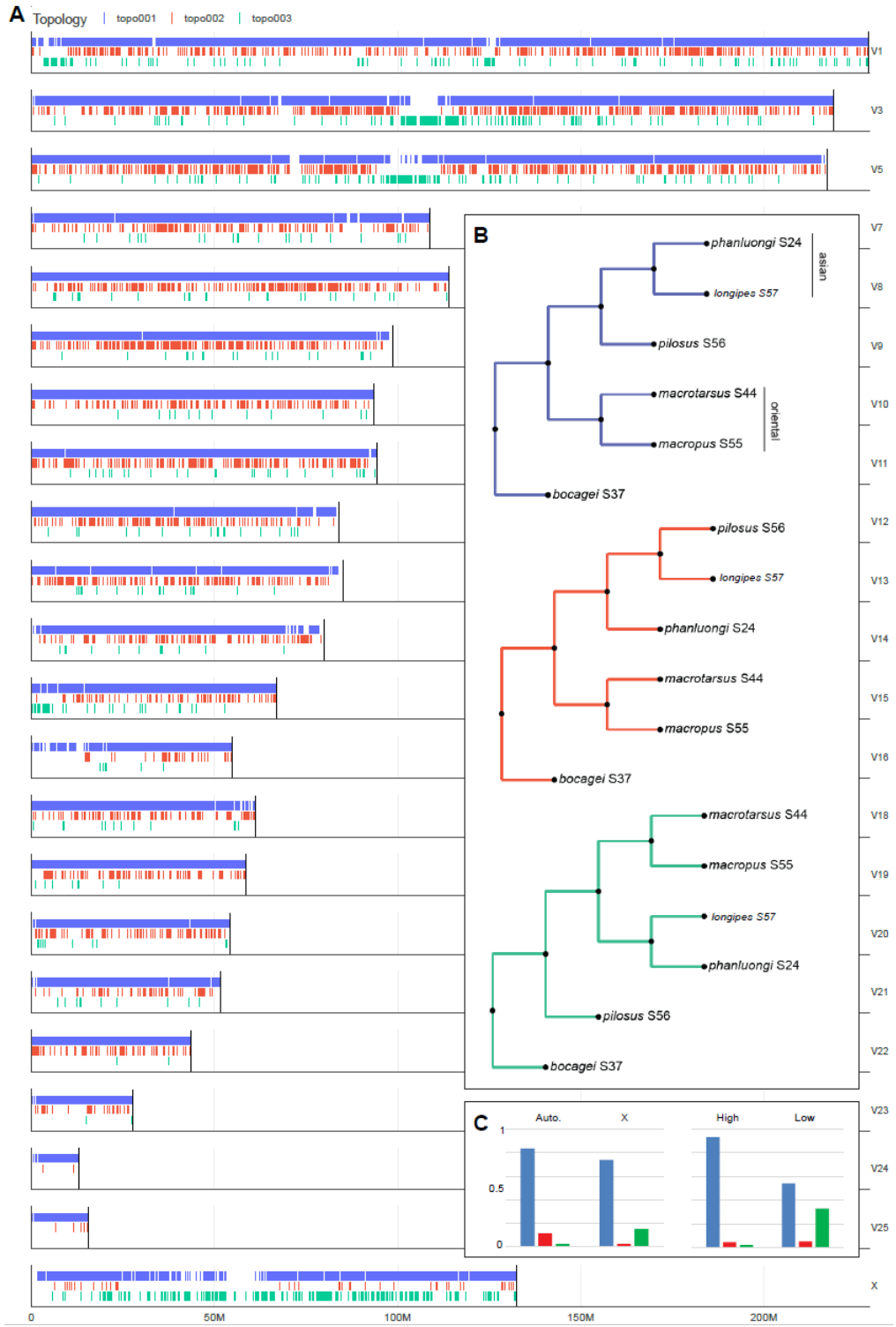

Figure S15: Genome-wide phylogenomic signal to determine the position of *M. pilosus*, related to Figure 3. A) Genome-wide distribution of topologies shown in B). C) shows the frequency of each topology on the autosomes and X and in high and low recombining regions.

Figure S16: Phylogenomic discordance, related to Figure 3. Topological frequency is calculated comparing the Autosomes and X and comparing low and high recombining regions. Average values of f(*D*), alpha and ibl per clade.

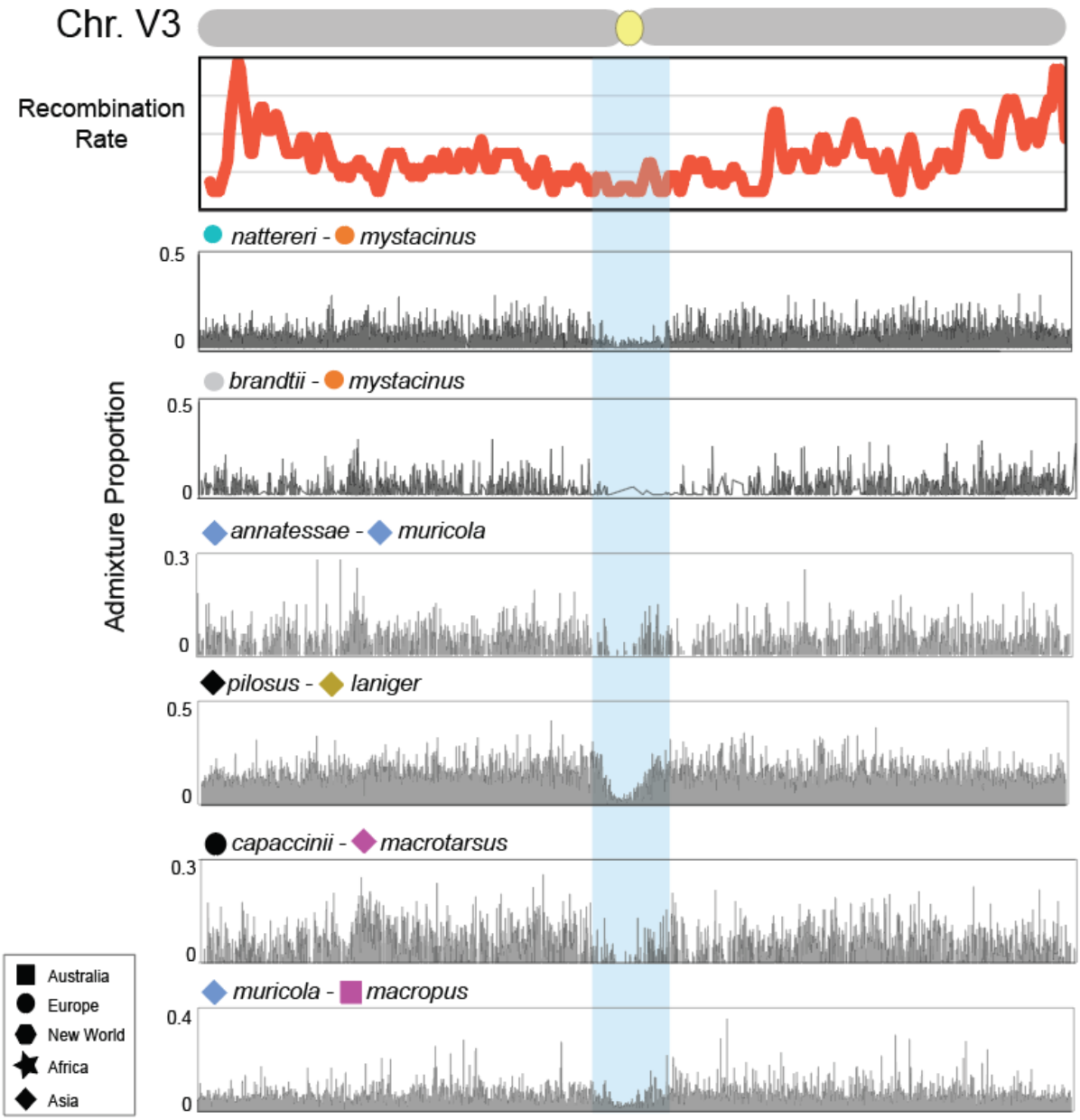

Figure S17: The f(*D*) statistic calculated across chromosome V3 for various species pairs, related to Figure 4. Introgression is evident along chromosome arms while low recombining pericentromeric regions are relatively devoid of signal consistent with introgression.

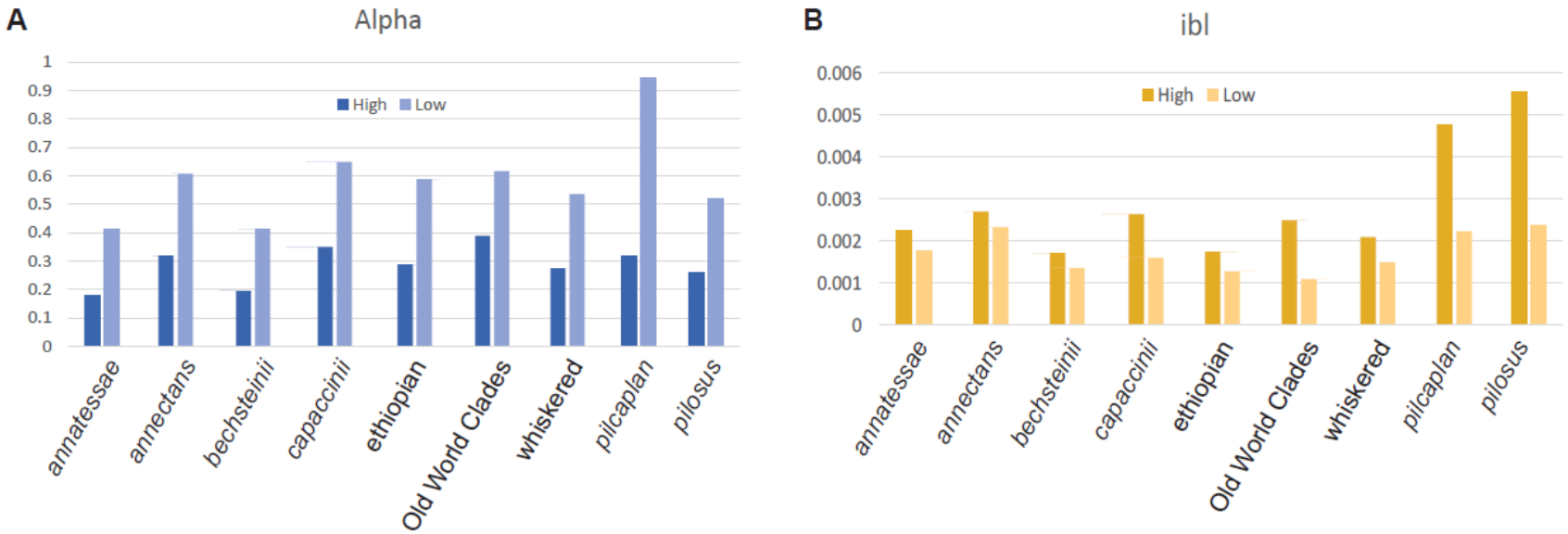

Figure S18: Distribution of alpha and internal branch length (ibl) in regions of high and low recombination, related to Figure 4.

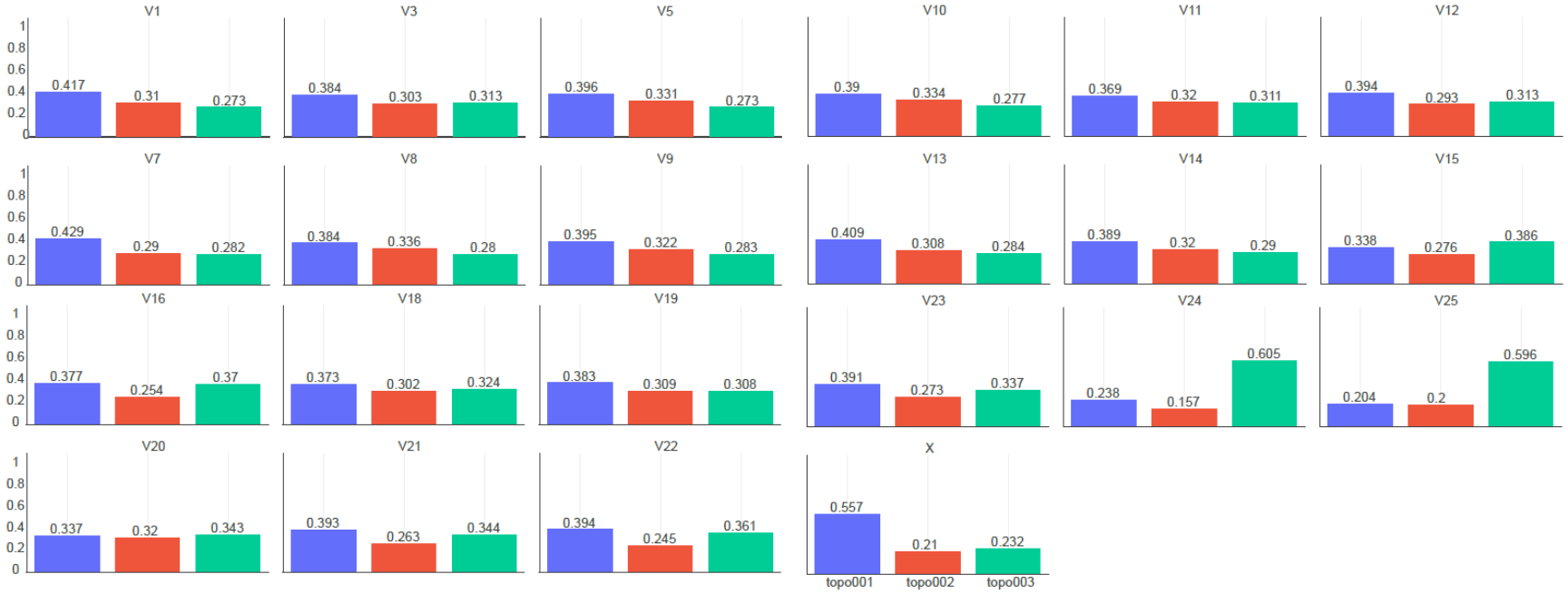

Figure S19: Topology frequency on each chromosome representing within clade relationships among species present at swarming sites, related to Figure 5.

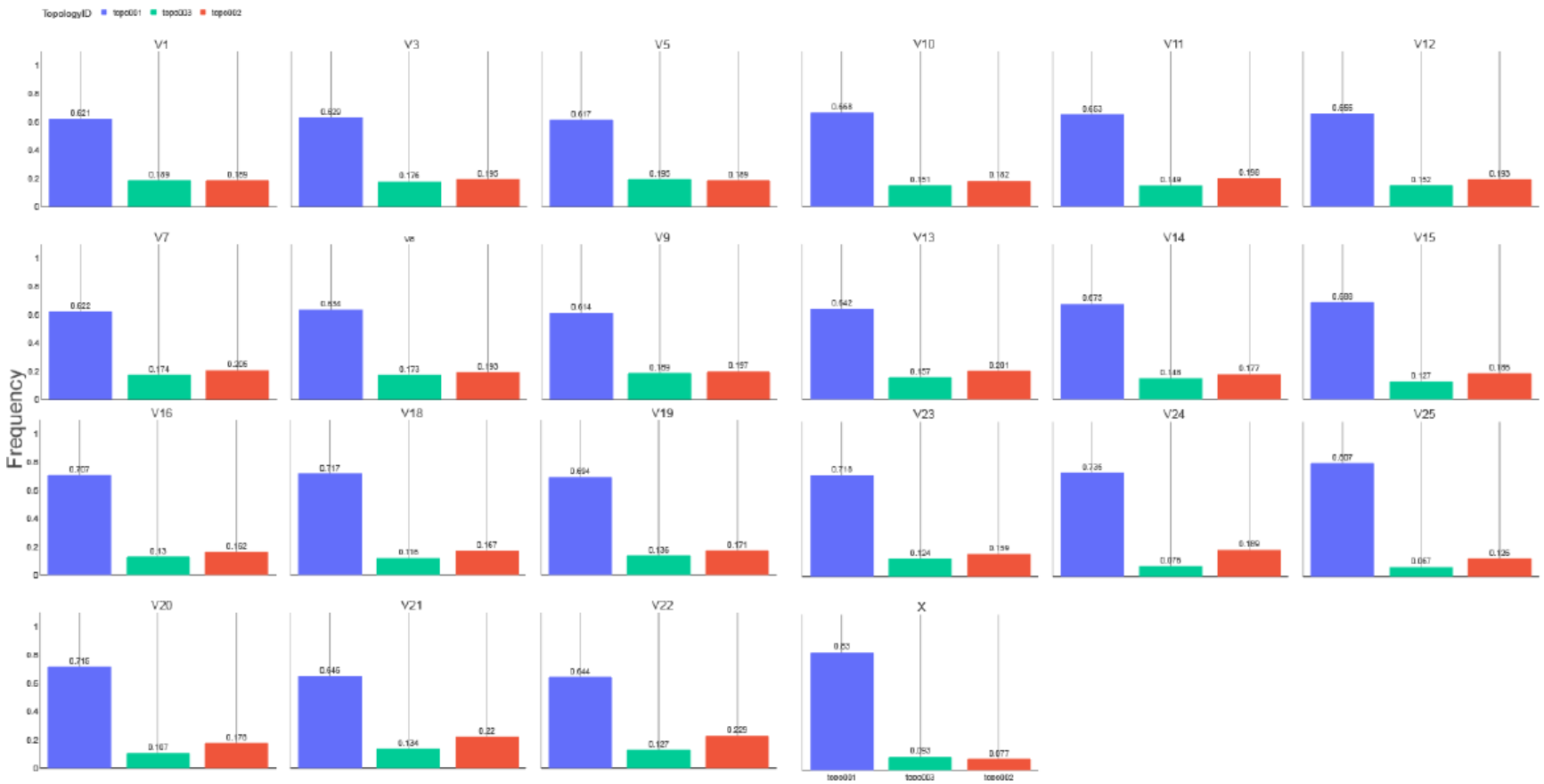

Figure S20: Topology frequency on each chromosome representing between clade relationships for *M. brandtii, M. mystacinus* and *M. alcathoe* at swarming sites, related to Figure 5.

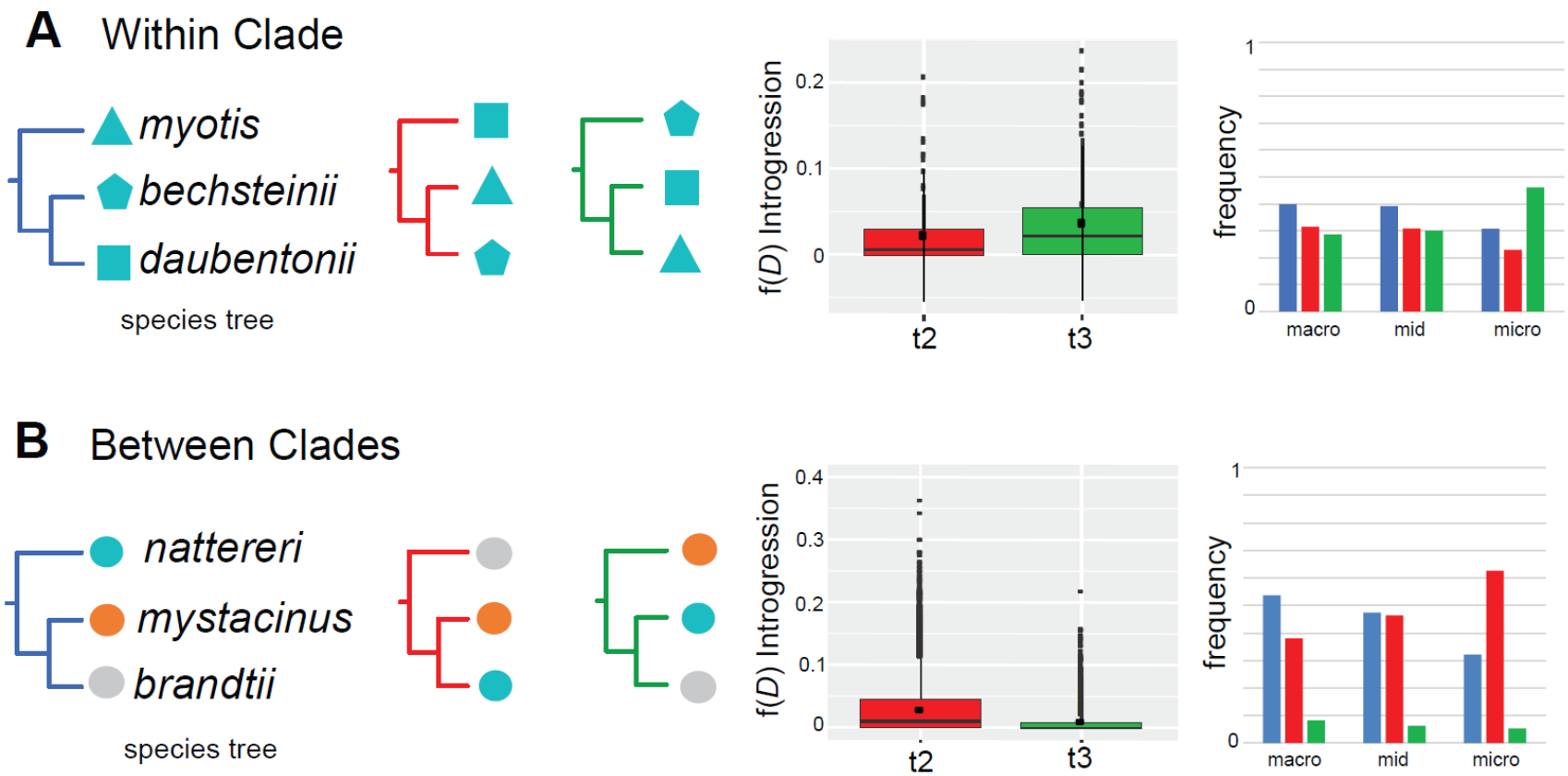

Figure S21: Introgressed topologies with the highest f(*D*) values are the most enriched on microchromosomes, related to Figure 6.

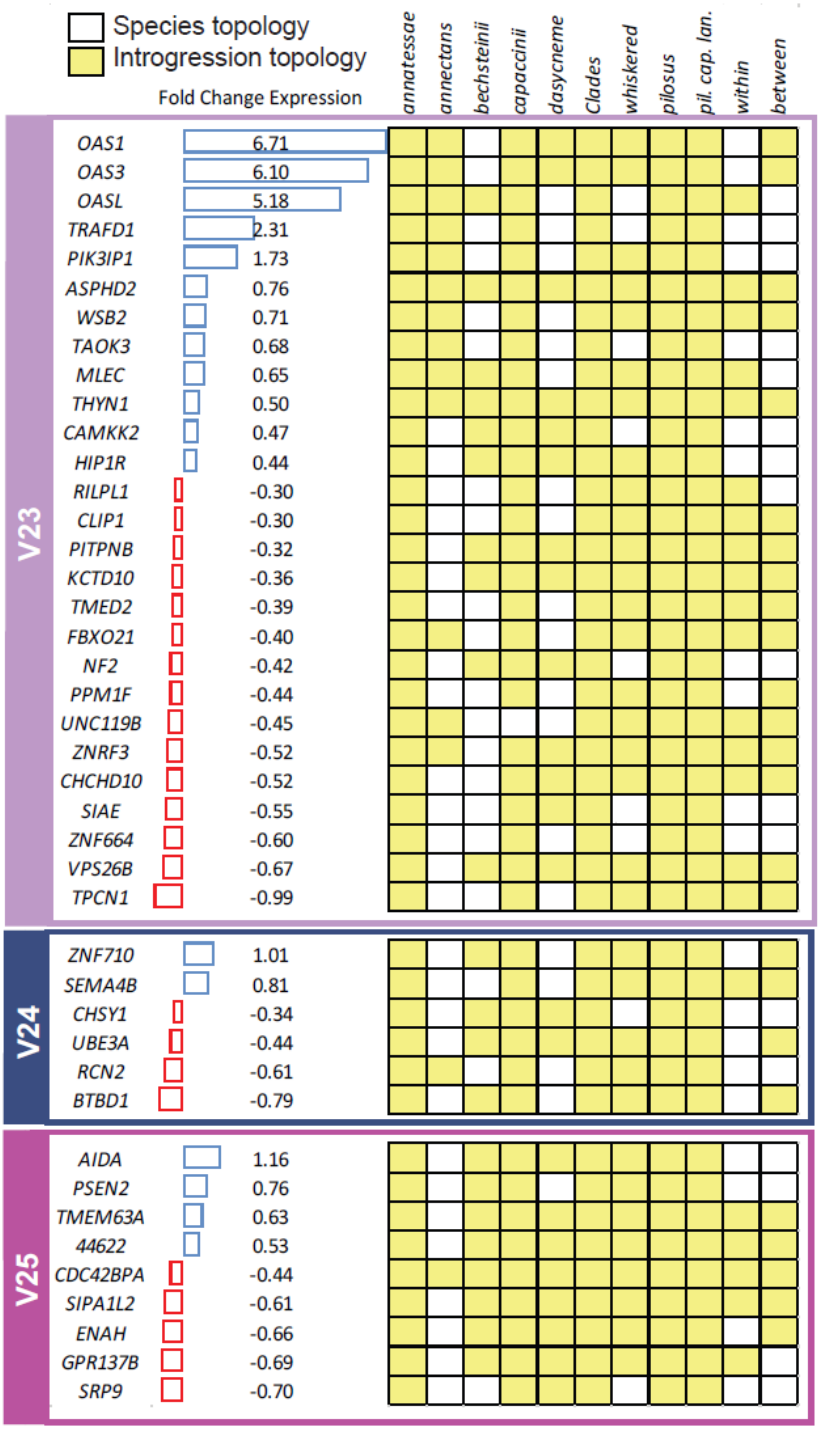

Figure S22: Genes that are differentially expressed in response to viral challenges in *M. daubentonii* were among the most frequently introgressed across microchromosomes, related to Figure 6.

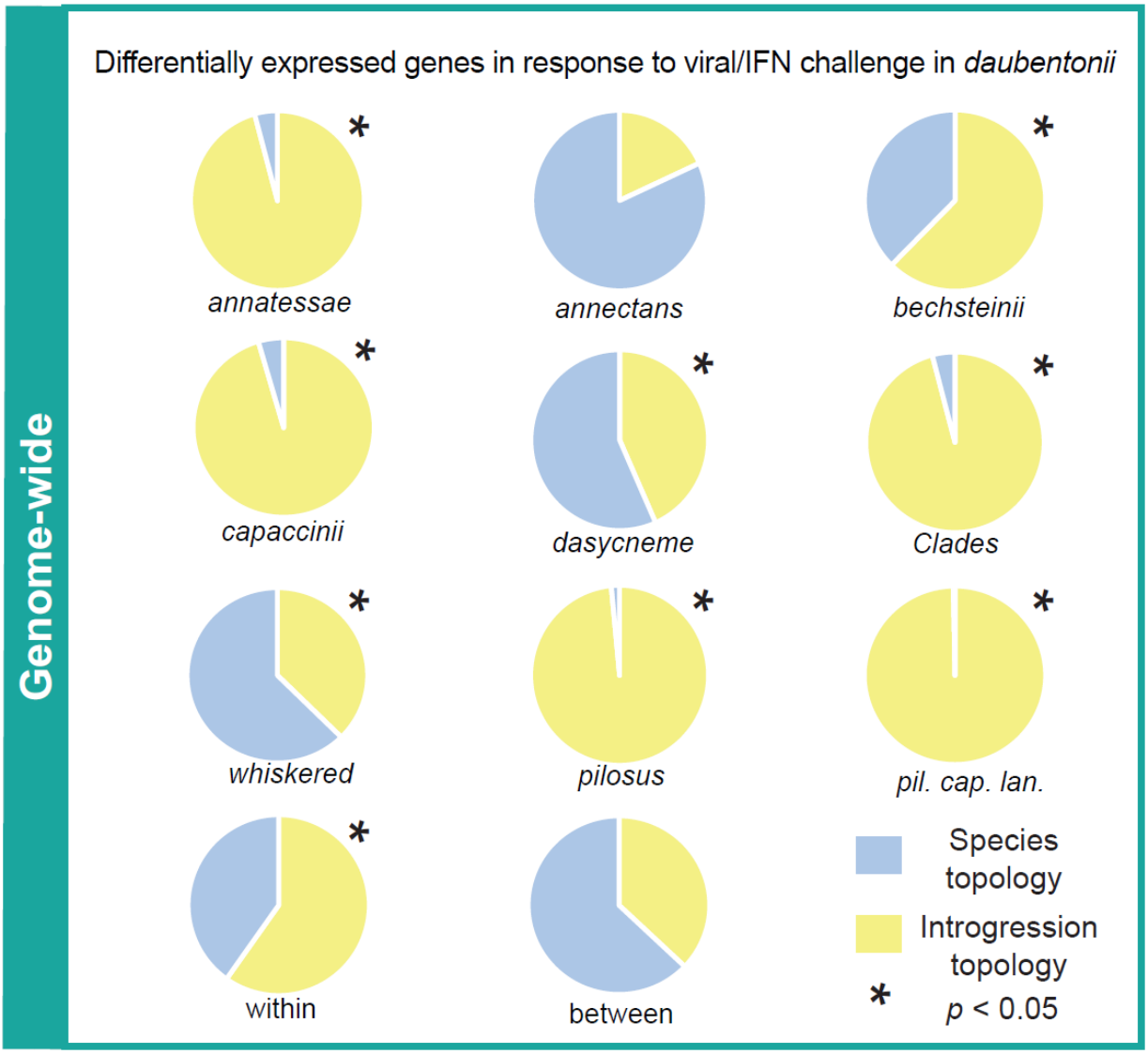

Figure S23: Significant overlap between introgressed genomic windows and genes that are differentially expressed in response to viral challenges in *M. daubentonii*, related to Figure 6.

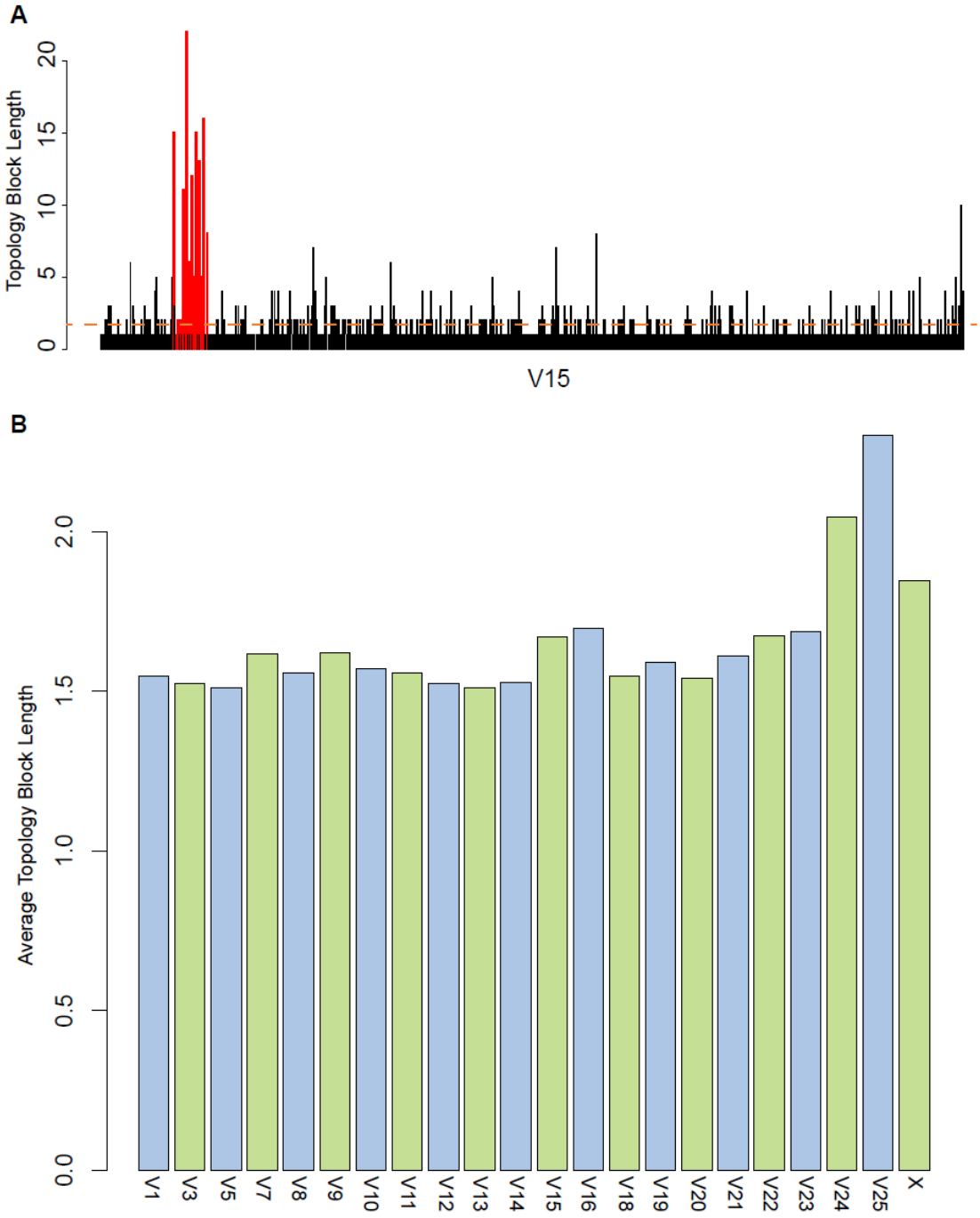

Figure S24: Plots of topology block length (=number of consecutive identical topologies) along chromosomes for the red topology uniting *M. myotis* and *M. daubentonii*, related to Figure 6. A) shows topology block length along chromosome V15. B) Microchromosomes V24 and V25 also exhibit elevated topology block lengths.

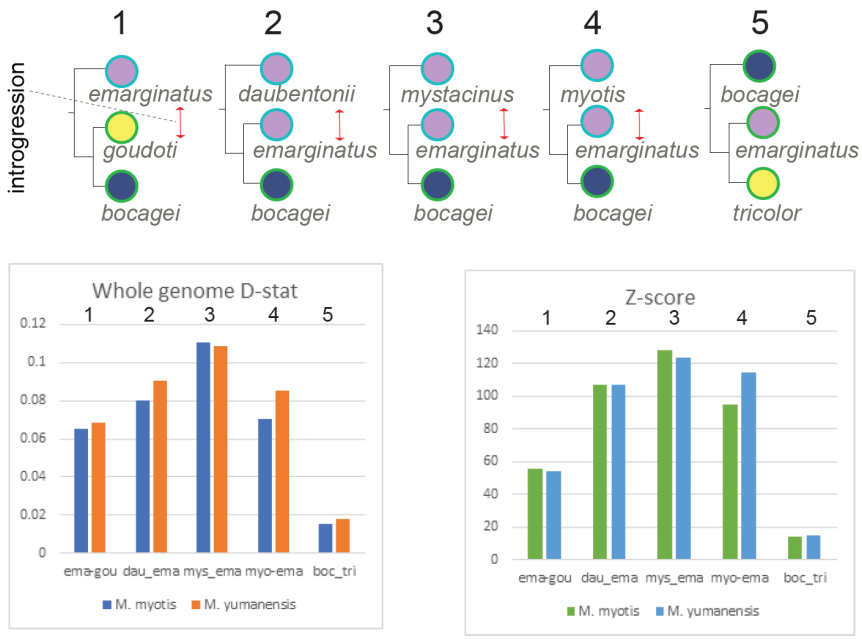

Figure S25: No impact of reference bias on whole genome tests of introgression, related to Figures 4, 5 and 6. *D*-statistics and Z-scores derived from data mapped to the *M. myotis* reference genome or the *M. yumanensis* genome are highly similar indicating the absence of reference bias

Table S1: Sample Information, related to Figure 1. Voucher or sample name, source and sampling locality for each sample used in this study. Categorization of broad scale species distributions as either tropical or temperate or spanning both. Abbreviations in sample source correspond to MHNG – Natural History Museum of Geneva, FMNH – Field Museum of Natural History Chicago, ZMMU – Zoological Museum Moscow Lomonosov State University, ROM – Royal Ontario Museum, EBD –Estacion Biologica de Doñana, AGS – Antonio Guillen-Servant, CMF – Charles M. Francis, SJP – Sebastien J. Puechmaille, MR – Manuel Ruedi

Voucher or Sample Name	Species	Sequencing Sample Number	Source	Locality	Clade
M2148	*latirostris*	S27	MHNG 1998.057	Taïwan.	
unknown	*spp.*	S37	MR		New World
M941	*alcathoe*	S26	MHNG 1828.073	Switzerland.	whiskered
M1575	*alcathoe*	S49	MHNG 1970.099	France.	whiskered
M803	*davidii*	S5	MHNG 1807.035	Greece	whiskered
M1993	*mystacinus*	S20	MHNG 1991.045	Switzerland.	whiskered
FMNH151200	*bocagei*	S42	FMNH	Tanzania	ethiopian
MZ004	*bocagei*	S37	MHNG 1971.027	Mozambique.	ethiopian
FMNH172095	*goudoti*	S45	MR/ FMNH	Madagascar.	ethiopian
FMNH173041	*goudoti*	S51	MR/ FMNH	Madagascar.	ethiopian
TM39421	*welwitschii*	S23	MR/ Transvaal Museum	South Africa.	ethiopian
FMNH144313	*welwitschii*	S47	MR/ FMNH	Uganda.	ethiopian
M733	*emarginatus*	S13	MHNG 1807.040	Greece.	ethiopian
MZ425	*tricolor*	S8	MHNG 1971.030	Mozambique.	ethiopian
TM40300	*tricolor*	S32	MR/ Transvaal Museum	South Africa.	ethiopian
Mdas1	*dasycneme*	S22	MHNG 1805.052	The Netherlands.	ethiopian
M1606	*laniger*	S57	MHNG 1981.074	India.	asian
AG 950116.6	*cf laniger*	S19	AG/ SMF 86179	Laos.	asian
M629	*laniger*	S50	MR	Taiwan.	asian
M1637	*siligorensis*	S31	MHNG 1981.073	India.	asian
N194	*alticraniatus*	S41	MHNG 1956.089	Laos.	asian
S175154	*phanluongi*	S24	MR/ ZMMU		asian
CMF960418.17	*pilosus*	S10	CMF	Laos.	asian
M2065	*pilosus*	S56	MR	India.	asian
CMF960522.46	*macrotarsus*	S20	CMF	Borneo.	oriental
EAR122	*macrotarsus*	S44	MR	Philippines.	oriental
M	*macropus*	S55	MR	Australia.	oriental
CMF960523.40	*horsfieldii*	S12	CMF	Borneo.	oriental

Voucher or Sample Name	Species	Sequencing Sample Number	Source	Locality	Clade
M1551	*horsfieldii*	S28	MHNG 1970.049	Malaysia.	oriental
M1184	*horsfieldii*	S2	MHNG 1926.038	Laos.	oriental
LRH3168	*browni*	S39	MR	Philippines.	oriental
Mca1	*capaccinii*	S34	MHNG 1805.050	Italy.	oriental
AGS980326.44	*montivagus*	S11	AGS	Laos.	muricola
M1208	*indochinensis*	S17	MHNG 1926.043	Laos.	muricola
CMF960408.3	*federatus*	S29	CMF/ROM 106389	Laos.	muricola
M1200	*annatessae*	S7	MHNG 1926.044	Laos.	muricola
M1165	*ater*	S9	MHNG 1926.036	Laos.	muricola
M1569	*muricola*	S30	MHNG 1970.064	Malaysia.	muricola
M1600	*muricola*	S40	MHNG 1972.084	Indonesia.	muricola
M2152	*secundus*	S25	MHNG 1998.058	Taïwan.	muricola
CMF960406.5	*annectans*	S35	CMF/ ROM 106376	Laos	muricola
M2139	*frater*	S21	MHNG 1998.053	Taïwan.	Large *Myotis* & others
M2163	*soror*	S15	MHNG 1998.05	Taïwan.	Large *Myotis* & others
M2009	*bechsteinii*	S18	MHNG 1991.067	Switzerland.	Large *Myotis* & others
M2187	*daubentonii*	S24	MHNG 1999.098	Switzerland.	Large *Myotis* & others
M301	*daubentonii nathalinae*	S54	MR	Spain	Large *Myotis* & others
M303	*daubentonii nathalinae*	S52	MR	Spain.	Large *Myotis* & others
EBD25765	*escalerai*	S36	EBD	Spain	Large *Myotis* & others
M2096	*crypticus*	S38	MHNG 1996.094	Switzerland.	Large *Myotis* & others
M764	*nattereri*	S33	MHNG 1807.049	Greece.	Large *Myotis* & others
MM4SA	*punicus*	S1	MHNG 1805.092	Italy.	Large *Myotis* & others
Mb203	*blythii*	S3	MHNG 1805.026	Kyrgyzstan.	Large *Myotis* & others
631D	*blythii*	S14	MHNG 1805.037	Switzerland.	Large *Myotis* & others
M867	*blythii*	S6	MHNG 1807.099	Greece.	Large *Myotis* & others
Mb3	*blythii*	S4	MHNG 1805.041	Spain.	Large *Myotis* & others
SP.C.47	*blythii*	S43	SJP	Iran	Large *Myotis* & others
SP.C.48	*blythii*	S48	SJP	Iran	Large *Myotis* & others
Mchin1	*ancilla*	S53	MR	China	Large *Myotis* & others

Table S2: Mapping Statistics, related to Figure 1.

Voucher or Sample Name	Species	Sequencing Sample Number	% Reference Covered	reads mapped	mean coverage
M2148	*latirostris*	S27	78.6	94.56%	25
unknown	*spp.*	S37	79.6	96.33%	12
M941	*alcathoe*	S26	82.1	97.68%	16
M1575	*alcathoe*	S49	84.4	97.44%	26
M803	*davidii*	S5	85	98.51%	23
M1993	*mystacinus*	S20	84.8	96.86%	22
FMNH144313	*welwitschii*	S47	83.1	95.94%	18
MZ004	*bocagei*	S37	84.8	97.17%	29
FMNH172095	*goudoti*	S45	81.5	95.22%	12
FMNH173041	*goudoti*	S51	84.8	96.80%	19
TM39421	*welwitschii*	S23	83.3	97.77%	17
FMNH151200	*bocagei*	S42	84	95.01%	19
M733	*emarginatus*	S13	86.1	98.32%	25
MZ425	*tricolor*	S8	85.4	97.52%	21
TM40300	*tricolor*	S32	86.2	98.11%	27
Mdas1	*dasycneme*	S22	79.5	98.70%	20
M1606	*laniger*	S57	85	98.78%	18
AG950116.6	*laniger*	S19	85.6	97.27%	23
M629	*laniger*	S50	85.8	98.33%	26
M1637	*siligorensis*	S31	84.8	97.39%	18
N194	*alticraniatus*	S41	86.6	98.29%	29
S175154	*phanluongi*	S24	81.3	97.45%	16
CMF960418.17	*pilosus*	S10	85.9	98.56%	24
M2065	*pilosus*	S56	86.1	98.68%	27
CMF960522.46	*macrotarsus*	S20	83	97.69%	14
EAR122	*macrotarsus*	S44	83.8	96.5%	16
M	*macropus*	S55	84.5	98.84%	20
CMF960523.40	*horsfieldii*	S12	86.1	97.91%	25

Voucher or Sample Name	Species	Sequencing Sample Number	% Reference Covered	reads mapped	mean coverage
M1551	*horsfieldii*	S28	83.5	97.01%	15
M1184	*horsfieldii*	S2	86.6	98.16%	28
LRH3168	*browni*	S39	83.9	96.62%	19
Mca1	*capaccinii*	S34	82.2	97.98%	13
AGS980326.44	*montivagus*	S11	85.2	97.63%	24
M1208	*indochinensis*	S17	85.4	97.06%	25
CMF960408.3	*federatus*	S29	85.7	97.62%	27
M1200	*annatessae*	S7	85.1	98.17%	20
M1165	*ater*	S9	85.9	98.04%	29
M1569	*muricola*	S30	84.9	96.57%	23
M1600	*muricola*	S40	84.6	94.99%	20
M2152	*secundus*	S25	86.7	96.75%	27
CMF960406.5	*annectans*	S35	82.4	97.80%	12
M2139	*frater*	S21	86.5	96.04%	20
M2163	*soror*	S15	86.4	97.90%	17
M2009	*bechsteinii*	S18	89.5	98.97%	27
M2187	*daubentonii*	S24	88.6	98.31%	20
M301	*daubentonii nathalinae*	S54	88.9	99.01%	23
M303	*daubentonii nathalinae*	S52	89	98.96%	26
EBD25765	*escalerai*	S36	90.5	96.94%	23
M2096	*crypticus*	S38	91.4	98.30%	28
M764	*nattereri*	S33	90.9	98.23%	24
MM4SA	*punicus*	S1	94.1	99.18%	20
Mb203	*blythii*	S3	94.1	98.86%	23
631D	*blythii*	S14	94.2	98.71%	24
M867	*blythii*	S6	93.5	99.35%	18
Mb3	*blythii*	S4	94.2	99.11%	22
SP.C.47	*blythii*	S43	93.3	98.64%	17
SP.C.48	*blythii*	S48	89.2	99.34%	17
Mchin1	*ancilla*	S53	93.1	98.44%	25

Table S3: Quast summary of difference between the original *Myotis myotis* assembly (HLmyoMyo6) and the improved assembly (Myotismyotis_assembly_V2), related to the improved *Myotis myotis* assembly described in the main text.

	HLmyoMyo	Myotismyotis_assembly_V2
# contigs	92	55
Largest contig	223369599	228434895
Total Length	2003238046	2003245946
GC%	43.11	43.11
N50	94448911	108770286
N75	74216526	79764552
L50	7	6
L75	12	12
# N's per 100kbp	1468.17	1468.56

Table S4: Species composition for each subclade examined in the analysis of genome-wide phylogenomic signal, related to Figure 3.

annatessae	***annectans***	***bechsteinii***	***capaccinii***	**ethiopian**	**Old World Clades**	**whiskered**	***pilcaplan***	***pilosus***
bocagei S37	*soror S15*	*bocagei S37*	*bocagei S37*	*latirostris S27*	*latirostris S27*	*latirostris S27*	*bocagei S37*	*bocagei S37*
muricola S30	*frater S21*	*bechsteinii S18*	*capaccinii S34*	*tricolor S32*	*laniger S19*	*mystacinus S20*	*capaccinii S34*	*macropus S55*
ater S9	*annectans S35*	*daubentonii S24*	*macropus S55*	*welwitschii S23*	*macropus S55*	*alcathoe S49*	*laniger S19*	*macrotarsus S44*
muricola S40	*secundus S25*	*ancilla S53*	*macrotarsus S20*	*bocagei S37*	*macrotarsus S44*	*brandtii*	*pilosus S56*	*pilosus S56*
federatus S29	*muricola S30*	*myotis*	*phanluongi S24*	*emarginatus S13*	*muricola S30*	*bocagei S37*		*phanluongi S24*
montivagus S11	*bocagei S37*	*soror S15*	*alticraniatus S41*	*dasycneme S22*	*montivagus S11*	*myotis*		*laniger S57*
annatessae S7		*frater S21*			*myotis*			
					ancilla S53			
					bocagei S37			

Table S5: Detailed breakdown of results for genome wide *D*-statistic tests, related to Figure 4. Trees were analyzed in the format (((H1, H2), H3,) Outgroup) where the outgroup was *S. latirostris* for all tests. A Z score above 3 is considered significant.

Reference genome	H1	H2	H3	nABBA	nBABA	Dstat	jackEst	SE	Z
Myotis myotis	MZ004_bocagei_S37	**M733_emarginatus_S13**	**M2187_daubentonii_S24**	1791427	1511330	0.084807	0.084807	0.00079	**107.3416**
Myotis yumanensis	MZ004_bocagei_S37	**M733_emarginatus_S13**	**M2187_daubentonii_S24**	1711426	1427716	0.090378	0.090378	0.000843	**107.2569**
Myotis myotis	MZ004_bocagei_S37	**M733_emarginatus_S13**	**myo_BROAD**	1800187	1563127	0.070484	0.070484	0.00074	**95.21591**
Myotis yumanensis	MZ004_bocagei_S37	**M733_emarginatus_S13**	**myo_BROAD**	1733777	1460703	0.085483	0.085483	0.000746	**114.6314**
Myotis myotis	MZ004_bocagei_S37	**M733_emarginatus_S13**	**M1993_mystacinus_S20**	1627722	1303891	0.110462	0.110462	0.000861	**128.308**
Myotis yumanensis	MZ004_bocagei_S37	**M733_emarginatus_S13**	**M1993_mystacinus_S20**	1548282	1244630	0.108722	0.108722	0.000881	**123.4457**
Myotis myotis	MZ004_bocagei_S37	**fmnh172095_goudoti_S45**	**M733_emarginatus_S13**	2226221	1954903	0.064891	0.064891	0.001166	**55.66637**
Myotis yumanensis	MZ004_bocagei_S37	**fmnh172095_goudoti_S45**	**M733_emarginatus_S13**	2135239	1861688	0.06844	0.06844	0.001266	**54.08118**
Myotis myotis	**TM40300_tricolor_S32**	M733_emarginatus_S13	**MZ004_bocagei_S37**	1981908	2042725	-0.01511	-0.01511	0.001075	**-14.0531**
Myotis yumanensis	**TM40300_tricolor_S32**	M733_emarginatus_S13	**MZ004_bocagei_S37**	1895093	1963687	-0.01778	-0.01778	0.001175	**-15.128**
Myotis myotis	myo_BROAD	**M2187_daubentonii_S24**	**S175154_phanluongi_S24**	2058223	1844105	0.054869	0.054869	0.001072	**51.19208**
Myotis myotis	M2009_bechsteinii_S18	**M2187_daubentonii_S24**	**myo_BROAD**	2580187	2536752	0.008488	0.008488	0.002327	**3.648049**
Myotis myotis	**CMF960522_46_macrotarsus_S20**	M2009_bechsteinii_S18	**M1569_muricola_S30**	2926327	3861014	-0.13771	-0.13771	0.001369	**-100.559**
Myotis myotis	**M2009_bechsteinii_S18**	M2096_nattereri_S38	**Mbrandtii**	1202345	1248347	-0.01877	-0.01877	0.000794	**-23.6339**
Myotis myotis	**M2187_daubentonii_S24**	M2096_nattereri_S38	**M1993_mystacinus_S20**	1394982	1545713	-0.05126	-0.05126	0.000799	**-64.1663**
Myotis myotis	**M1993_mystacinus_S20**	Mbrandtii	**M2096_nattereri_S38**	2184190	3099853	-0.17329	-0.17329	0.002389	**-72.5429**
Myotis myotis	**M2139_frater_S21**	M2009_bechsteinii_S18	**CMF960406_5_annectans_S35**	2760696	3263672	-0.08349	-0.08349	0.002849	**-29.3023**
Myotis myotis	**M1993_mystacinus_S20**	M941_alcathoe_S26	**Mbrandtii**	2430561	2617513	-0.03703	-0.03703	0.001214	**-30.496**

Reference genome	H1	H2	H3	nABBA	nBABA	Dstat	jackEst	SE	Z
Myotis myotis	**CMF960522_46_macrotarsus_S20**	S175154_phanluongi_S24	**Mca1_capaccinii_S34**	3473250	4084785	-0.08091	-0.08091	0.00315	**-25.6831**
Myotis myotis	**M941_alcathoe_S26**	Mbrandtii	**Mdas1_dasycneme_S22**	2214338	3236368	-0.1875	-0.1875	0.00342	**-54.82**
Myotis myotis	**M1993_mystacinus_S20**	Mbrandtii	**Mdas1_dasycneme_S22**	2121574	3071673	-0.18295	-0.18295	0.002391	**-76.5191**
Myotis myotis	M733_emarginatus_S13	**Mdas1_dasycneme_S22**	**M2009_bechsteinii_S18**	2507335	2422351	0.017239	0.017239	0.001189	**14.49878**
Myotis myotis	**M2187_daubentonii_S24**	M2096_nattereri_S38	**Mdas1_dasycneme_S22**	1560422	1696782	-0.04186	-0.04186	0.000738	**-56.7437**
Myotis myotis	M733_emarginatus_S13	**Mdas1_dasycneme_S22**	**M1993_mystacinus_S20**	2131851	2029572	0.024578	0.024578	0.000942	**26.09706**
Myotis myotis	myo_BROAD	M733_emarginatus_S13	M1993_mystacinus_S20	2532201	2527665	0.000896	0.000896	0.001001	0.895467
Myotis myotis	M2009_bechsteinii_S18	**M2187_daubentonii_S24**	**M2096_nattereri_S38**	2621507	2579505	0.008076	0.008076	0.002248	**3.592021**
Myotis myotis	**M629_laniger_S50**	CMF960522_46_macrotarsus_S20	**M2065_pilosus_S56**	2361436	7045984	-0.49796	-0.49796	0.002534	**-196.503**
Myotis myotis	**M1569_muricola_S30**	M1208_indochinensis_S17	**M1200_annatessae_S7**	3455060	3730538	-0.03834	-0.03834	0.00132	**-29.0523**
Myotis myotis	**M2187_daubentonii_S24**	M2009_bechsteinii_S18	**myo_BROAD**	2536800	2581340	-0.0087	-0.0087	0.002334	**-3.72829**
Myotis myotis	**M2139_frater_S21**	M2187_daubentonii_S24	**M2065_pilosus_S56**	2650991	3062319	-0.07199	-0.07199	0.001695	**-42.4712**
Myotis myotis	M1569_muricola_S30	**M1208_indochinensis_S17**	**CMF960406_5_annectans_S35**	2093563	1918718	0.043577	0.043577	0.000709	**61.43691**
Myotis myotis	**M2096_nattereri_S38**	**M2187_daubentonii_S24**	**M733_emarginatus_S13**	**1610340**	**1590837**	**0.006092**	**0.006092**	**0.000795**	**7.668013**

Table S6: Results of the QuIBL analysis, related to Figure 4. The table shows the proportion of variation in discordant topologies explained by ILS alone or a combination of ILS and introgression. The difference in BIC estimates (delta) for each model indicates that the model with introgression and ILS (preferred at delta ≥-10) is the best fit for all relationships analyzed. Old World Clades refers to the relationship among the Muricola, Large Myotis, Asian, and Oriental clades shown in Figure 1. *pil.-cap.-lan.* refers to the relationship among *pilosus*, *capaccinii,* and *laniger*. Non-species trees are color-coded to correspond with data displayed in Figure 1.

Clade	non-species topology	tree	ILS	Introgression + ILS	delta
annatessae	topo002	*(annatessae, (indochinensis, muricola))*	0%	100%	-13383
	topo001	*indochinensis, (muricola ,annatessae))*	0%	100%	-17245
annectans	topo003	*(annectans, (frater, muricola))*	0%	100%	-995
	topo002	*(frater, (annectans, muricola))*	0%	100%	-3319
bechsteinii	topo002	*(bechsteinii, (daubentonii, myotis))*	0%	100%	-9038
	topo003	*(daubentonii, (bechsteinii, myotis))*	0%	100%	-9045
capaccinii	topo001	*(phanluongi, (capaccinii, macrotarsus))*	0%	100%	-30065
	topo002	*(macrotarsus, (capaccinii, phanluongi))*	0%	100%	-5825
dasycneme	topo004	*(mystacinus, (alcathoe, (dasycneme, bocagei)))*	0%	100%	-299
	topo002	*(bocagei, (dasyceneme, (mystacinus, alcathoe)))*	0%	100%	-44060
Clades	topo003	*(muricola, (myotis, macrotarsus))*	0%	100%	-9122
	topo001	*(myotis, (macrotarsus, muricola))*	0%	100%	-17445
whiskered	topo004	*(alcathoe, (mystacinus, brandtii))*	0%	100%	-4761

	topo006	*(mystacinus, alcathoe, brandtii))*	0%	100%	-4474
pil. cap. lan.	topo003	*(laniger, (capaccinii,pilosus))*	73%	27%	33
	topo001	*capaccinii, ((pilosus, laniger))*	0%	100%	-33039
pilosus	topo001	*(macropus, (pilosus, laniger))*	0%	100%	-32580
	topo005	*(pilosus, (macropus, laniger))*	28%	72%	-174

Table S7: Studies reporting species presence at swarming sites across Europe [S2-16], related to Figure 5. Although *M. myotis* and *M. blythii* are thought to use a lekking mating behavior

Paper	Schunger et al (2004)	Dundarova (2018)	Rivers et al (2006)	Parsons et al (2003)	Piksa et al (2011)	Suba et al (2008)	Schaik et al (2015)	Bogdanowicz et al 2012	Suba et al (2011)	Glover and Altringham (2008)	Schmidbauer and Denzinger (2019)	Pocora et al (2012)	Dekeukeleire et al (2016)	Thomas and Davison (2020)	Ignaczak et al (2019)
Country	Bulgaria	Bulgaria	UK	UK	Poland	Latvia	Netherlands	Poland	Latvia	UK	Germany	Romania	Belgium and Netherlands	Wales	Poland
myotis	x	x			x		x				x	x	x		x
blythii	x	x													
bechsteinii	x	x		x	x		x					x	x	x	x
nattereri/crypticus	x	x	x	x	x	x				x	x	x	x	x	x
daubentonii	x	x	x	x	x	x	x		x	x		x			x
brandtii	x	x	x	x	x	x	x	x	x	x		x	x	x	x
alcathoe	x	x			x			x							
mystacinus		x	x	x	x	x	x	x		x		x	x	x	
emarginatus	x	x					x						x		
dasycneme					x	x	x		x				x		

Table S8: STRING enrichment analysis for an introgressed block on V15 which unites *M. myotis* and *M. daubentonii*, related to Figure 6. Enrichments are considered significant with an FDR value of ≥ 0.05.

Category	#term ID	term description	observed gene count	background gene count	strength	false discovery rate
Molecular Function	GO:0005149	interleukin-1 receptor binding	7	17	2.04	8.6E-09
Molecular Function	GO:0070851	Growth factor receptor binding	8	138	1.19	1.2E-04
Molecular Function	GO:0005126	Cytokine receptor binding	8	264	0.9	9.0E-03
KEGG Pathway	hsa04060	Cytokine-cytokine receptor interaction	7	282	0.82	3.6E-02
Reactome Pathway	HSA-446652	Interleukin-1 family signaling	7	136	1.13	2.4E-03
Reactome Pathway	HSA-9014826	Interleukin-36 pathway	3	6	2.12	4.6E-03

Table S9: Immunogenetic diversification mechanisms across the Tree of Life, related to Figure 6. Note that most of these mechanisms operate within the listed taxa. MHC allelic polymorphism has long been of interests to evolutionary biologists due to its function at the population level. Now adaptive immunogenetic introgression in *Myotis* bats appears to elevate such defense diversification strategies to the level of the multispecies community.

Taxa	Process	Genes Diversified	Evolutionary Facilitation	Mechanism
archaea/bacteria	adaptive anti-phage immunity	clustered regularly interspaced short palindromic repeats (CRISPR)	horizontal gene transfer	CRISPR/cas9 [S17]
arthropods	repertoire of pattern recognition receptors	down syndrome cell adhesion molecule (DSCAM)	exon family expansion	mutually exclusive alternative RNA exon splicing [S18]
jawless fishes	VLR repertoire diversification	variable lymphocyte receptors	copy-choice recombination	APOBEC family deaminases [S19]
jawed vertebrates	somatic cell gene rearrangement of lymphocyte antigen receptors	immunoglobulin, T cell receptor	horizontal transposon capture	recombination activating genes (RAG) [S20]
jawed vertebrates	antibody affinity maturation	immunoglobulin heavy and light chain variable genes	selection of controlled somatic hypermutation	activation induced cytidine deaminase (AID) [S21]
Bovidae	ultralong cattlebody knob diversification	third complementarity determining region (CDR3) of immunoglobulin heavy chain	bias for cysteine mutation, truncations in CDR3	activation induced cytidine deaminase (AID) [S22]
jawed vertebrates	allelic polymorphism	classical MHC antigen presentation	balancing selection, pathogen co-evolution	extreme allelic diversity in peptide binding – **Population** [S23]
***Myotis* bats**	tunable immunogenetic viral tolerance	interferons, antigen processing, anti-viral signaling	swarming, interspecific hybridization	adaptive immunogenetic introgression – **Genus Community**

Supplementary References

S1. Jebb, D., Huang, Z., Pippel, M., Hughes, G.M., Lavrichenko, K., Devanna, P., Winkler, S., Jermiin, L.S., Skirmuntt, E.C., Katzourakis, A., et al. (2020). Six reference-quality genomes reveal evolution of bat adaptations. Nature *583*, 578–584.

S2. Schunger, I., Dietz, C., Merdschanova, D., Merdschanov, S., Christov, K., Borissov, I., Staneva, S., and Petrov, B. (2004). Swarming of bats (Chiroptera, Mammalia) in the Vodnite Dupki cave (Central Balkan National Park, Bulgaria). Acta Zool. *56*, 323–330.

S3. Dundarova, H. (2018). Bat diversity in Lednitsata and Forgovskata dupka Caves: two potentially important swarming sites in Western Rhodopes Mts., Bulgaria. Acta Zool. Bulg. *70*, 139–142.

S4. Rivers, N.M., and Butlin R. K. Altringham, J.D. (2006). Autumn swarming behaviour of Natterer's bats in the UK: population size, catchment area and dispersal. Biol. Conserv. *127*, 215–226.

S5. Parsons, K.N., Jones, G., and Greenaway, F. (2003). Swarming activity of temperate zone microchiropteran bats: effects of season, time of night and weather conditions. J. Zool. *261*, 257–264.

S6. Piksa, K., Bogdanowicz, W., and Tereba, A. (2011). Swarming of Bats at Different Elevations in the Carpathian Mountains. Acta Chiropterologica *13*, 113–122.

S7. Šuba, J., Vintulis, V., and Pētersons, G. (2008). Late summer and autumn swarming of bats at Sikspārņu caves in Gauja National Park. Acta Univ. Latv *745*, 43–52.

S8. van Schaik, J., Janssen, R., Bosch, T., Haarsma, A.-J., Dekker, J.J.A., and Kranstauber, B. (2015). Bats Swarm Where They Hibernate: Compositional Similarity between Autumn Swarming and Winter Hibernation Assemblages at Five Underground Sites. PLoS One *10*, e0130850.

S9. Bogdanowicz, W., Piksa, K., and Tereba, A. (2012). Hybridization hotspots at bat swarming sites. PLoS One *7*, e53334.

S10. Suba, J., Vintulis, V., and Petersons, G. (2010). Body weight provides insights into the feeding strategy of swarming bats. Hystrix, the Italian *22*, 1.

S11. Glover, A.M., and Altringham, J.D. (2008). Cave selection and use by swarming bat species. Biol. Conserv. *141*, 1493–1504.

S12. Schmidbauer, P., and Denzinger, A. (2019). Social calls of *Myotis nattereri* during swarming: Call structure mirrors the different behavioral context. PLoS One *14*, e0221792.

S13. Pocora, I., Pocora, V., and Baltag, E. (2012). Swarming activity of bats at the entrance of Liliecilor cave from Rarău Mountains. Analele Ştiinţifice ale *58*, 151–158.

S14. Dekeukeleire, D., Janssen, R., Haarsma, A.-J., Bosch, T., and Van Schaik, J. (2016). Swarming behaviour, catchment area and seasonal movement patterns of the Bechstein's bats: implications for conservation. Acta Chiropt. *18*, 349–358.

S15. Ignaczak, M., Postawa, T., Lesiński, G., and Gottfried, I. (2019). The role of autumnal swarming behaviour and ambient air temperature in the variation of body mass in temperate bat species. Hystrix *30*, 65–73.

S16. Thomas, R.J., and Davison, S.P. (2022). Seasonal swarming behavior of *Myotis* bats revealed by integrated monitoring, involving passive acoustic monitoring with automated analysis, trapping, and video monitoring. Ecol. Evol. *12*, e9344.

S17. Jinek, M., Chylinski, K., Fonfara, I., Hauer, M., Doudna, J.A., and Charpentier, E. (2012). A Programmable Dual-RNA–Guided DNA Endonuclease in Adaptive Bacterial Immunity. Science *337*, 816–821.

S18. Watson, F.L., Püttmann-Holgado, R., Thomas, F., Lamar, D.L., Hughes, M., Kondo, M., Rebel, V.I., and Schmucker, D. (2005). Extensive diversity of Ig-superfamily proteins in the immune system of insects. Science *309*, 1874–1878.

S19. Pancer, Z., Amemiya, C.T., Ehrhardt, G.R.A., Ceitlin, J., Gartland, G.L., and Cooper, M.D. (2004). Somatic diversification of variable lymphocyte receptors in the agnathan sea lamprey. Nature *430*, 174–180.

S20. Hozumi, N., and Tonegawa, S. (1976). Evidence for somatic rearrangement of immunoglobulin genes coding for variable and constant regions. Proc. Natl. Acad. Sci. U. S. A. *73*, 3628–3632.

S21. Muramatsu, M., Kinoshita, K., Fagarasan, S., Yamada, S., Shinkai, Y., and Honjo, T. (2000). Class switch recombination and hypermutation require activation-induced cytidine deaminase (*AID*), a potential RNA editing enzyme. Cell *102*, 553–563.

S22. Wang, F., Ekiert, D.C., Ahmad, I., Yu, W., Zhang, Y., Bazirgan, O., Torkamani, A., Raudsepp, T., Mwangi, W., Criscitiello, M.F., et al. (2013). Reshaping antibody diversity. Cell *153*, 1379–1393.

S23. Zinkernagel, R.M., and Doherty, P.C. (1974). Restriction of in vitro T cell-mediated cytotoxicity in lymphocytic choriomeningitis within a syngeneic or semiallogeneic system. Nature *248*, 701–702.